

Mitigating the Curse of Detail: Scaling Arguments for Feature Learning and Sample Complexity

Noa Rubin¹, Orit Davidovich², and Zohar Ringel¹

¹Racah institute of Physics, Hebrew University, Jerusalem, Israel,

²IBM Research, Haifa, Israel.

December 10, 2025

Abstract

Two pressing topics in the theory of deep learning are the interpretation of feature learning mechanisms and the determination of implicit bias of networks in the rich regime. Current theories of rich feature learning, often appear in the form of high-dimensional non-linear equations, which require computationally intensive numerical solutions. Given the many details that go into defining a deep learning problem, this complexity is a significant and often unavoidable challenge. Here, we propose a powerful heuristic route for predicting the data and width scales at which various patterns of feature learning emerge. This form of scale analysis is considerably simpler than exact theories and reproduces the scaling exponents of various known results. In addition, we make novel predictions on complex toy architectures, such as three-layer non-linear networks and attention heads, thus extending the scope of first-principle theories of deep learning.

1 Introduction

There is a clear need for a better theoretical understanding of deep learning. However, efforts to construct such theories inevitably suffer from a “curse of details”. Indeed, since any choice of architecture, activation, data measure, and training protocol affects performance, finding a theory with true predictive power that accurately accounts for all those details is unlikely. One workaround is to focus on analytically tractable toy models, an approach that can often uncover interesting fundamental aspects. However, analytical tractability is a fragile, fine-tuned property; thus, a large explainability gap remains between such toy models and more complex data/architecture settings.

An alternative approach focuses on scaling properties of neural networks, which appear more robust. Two well-established examples are empirically predicting network performance by extrapolating learning curves using power laws Kaplan et al. [2020], Hestness et al. [2017], and providing theory-inspired suggestions for hyperparameter transfer techniques Yang et al. [2022], Bordelon et al. [2023]. Indeed, it is often the case Cardy [1996] that predicting scaling exponents is easier than predicting exact or approximate behaviors. As a simple toy model of this, consider the integral $\int_{-\infty}^{\infty} dx g(x/P)$. While $g(\cdot)$ needs to be fine-tuned for exact computations, a change of variable reveals a robust linear scaling with P for any $g(\cdot)$.

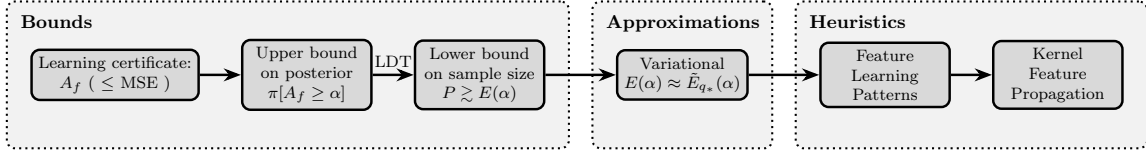


Figure 1: Logical flow of sample complexity derivation. **Bounds:** (i)-(iii) deriving lower bounds on sample complexity using LDT (Sec. 3). **Approximations:** (iv) approximating the intractable lower bound (Sec. 4), **Heuristics:** (v)-(vi) providing heuristic methods for manually computing the approximated bound (Sec. 5). Each section is composed of intermediate steps as detailed in the diagram.

This work focuses on scaling properties of feature learning. Feature learning, or, more generally, interpretability, have been studied extensively both from the practical and theoretical side. On the practical side, mechanistic interpretability Bereska and Gavves [2024] has provided us with statistical explanations for why some predictions are made and the underlying decision mechanisms. On the theory side, kernel-based approaches Aitchison [2019], Li and Sompolinsky [2021], Aitchison [2021], Seroussi et al. [2023a], Ariosto et al. [2022], Bordelon and Pehlevan [2022], Rubin et al. [2024, 2025], Ringel et al. [2025] and Saad and Solla type approaches Saad and Solla [1995], Arnaboldi et al. [2023], Bietti et al. [2022] (and their Bayesian counterparts Cui [2025]) allow us to solve simple non-linear teacher-student networks in the rich regime. However, our ability to capture more elaborate and compositional feature learning effects, such as those involving depth and emergence, is hampered by said analytical difficulties.

In this work, we introduce a novel framework addressing the challenging task of making first-principles predictions on sample complexity and feature learning effects in networks trained to equilibrium. The undeniable success of various deep learning models across diverse domains underscores the importance of theoretically predicting the conditions under which these models exhibit failure modes. Accordingly, a main focus of this work is lower-bounding sample complexity. Specifically, we aim to determine the scaling behavior of P_* , the threshold sample size at which learning becomes possible, as a function of input dimension, layer width, regularization, and parametrization choices (e.g., mean-field versus standard scaling).

Our Bayesian approach, capturing networks fully trained using SGLD ¹ Mandt et al. [2017], is described schematically in Fig. 1. It consists of the following steps: (i) we lower bound the test MSE by $(1 - A_f)^2$, where A_f is the alignment of output and target; (ii) we establish an upper bound on the probability to observe good learning (ie, strong alignment $A_f \geq \alpha \approx 1$) in the posterior using the negative-log-probability of the rare event of good learning in the prior; (iii) we leverage an *upper* bound on the prior to obtain a *lower* bound $E(\alpha)$ on the minimal sample size necessary for alignment of at least α ; (iv) we derive a variational approximation, $\tilde{E}_q(\alpha)$, for $E(\alpha)$ with an explicit formula using kernel-adaptation type approximations; (v) we propose *feature learning patterns* as heuristic variational probabilities q and choose such q that minimizes $\tilde{E}_q(\alpha)$; finally (vi) our fully analytic computation of $\tilde{E}_q(\alpha)$ further relies on heuristic scaling relations for how a feature amplified in one layer *propagates* to downstream layers.

Using the above, we re-derive, in a relatively straightforward manner, known results on two-layer networks: sample complexity benefits of rich learning and Grokking transitions. We demonstrate

¹which can be thought of as a proxy for SGD Mingard et al. [2020]

the power of this approach by expanding the scope of tractable models. Specifically, we study non-linear 3-layer networks in the rich regime and predict sample complexity, layer-wise location of learning, and scaling of the number of specializing neurons.

2 Setup

We consider here several types of feedforward networks, but, for the sake of clarity, we illustrate the main derivation on deep fully connected networks (FCNs) and, later, when we analyze specific problems, augment it for convolutional neural networks (CNNs) as needed. Our FCNs are defined by

$$f(x) = \sum_{i=1}^{N_{L-1}} w_i^L \sigma(h_i^{L-1}(x)), \quad \text{where } h_i^{l>1}(x) = \sum_{j=1}^{N_{l-1}} W_{ij}^l \sigma(h_j^{l-1}(x)), \quad h_j^1(x) = \sum_{k=1}^d W_{jk}^1 x_k, \quad (1)$$

where σ can be any activation function, and we refer to h_i^l 's as *pre-activations*. We consider Bayesian neural networks, as Bayesian descriptions are a commonly used proxy for network behavior after long-time stochastic training Wilson and Izmailov [2020], Wilson [2020], Naveh et al. [2021]. Alternatively, they represent an exact solution to Langevin dynamics with weight decay Welling and Teh [2011b]. We denote the target function by y and the training sample size by P , and assume training with Mean Squared Error (MSE) loss. The quadratic weight decay for each layer l is set to $\kappa N_{l-1}/\sigma_l^2$, where κ is the ridge parameter and $N_0 = d$ is the input dimension. This choice of weight decay results in a Gaussian prior distribution for the weights given by $W_{i,j}^l \sim \mathcal{N}(0, \sigma_l^2/N_{l-1})$ for $i = 1, \dots, N_l$, $j = 1, \dots, N_{l-1}$. The possible outputs f of such a network, given y and P , are then distributed according to the posterior:

$$\pi(f | y, P) = \frac{1}{Z} \exp \left(-\frac{1}{2\kappa} \sum_{\nu=1}^P [f(x_\nu) - y(x_\nu)]^2 \right) p_0(f), \quad (2)$$

where Z is the normalization constant, $\{x_\nu\}_{\nu=1}^P$ is the training dataset of size P , and $p_0(f)$ is the prior defined as $p_0(f) = \int d\Theta p(\Theta) \delta[f - f_\Theta]$, determined by the weight decay. Here, Θ is the collection of all network weights, and $p(\Theta)$ corresponds to the density of the prior weight distribution, which we take to be Gaussian with a diagonal covariance, representing quadratic weight decay, and f_Θ is the network architecture with weights Θ . We further set $p(\Theta)$ such that pre-activations are all $\mathcal{O}(1)$ under the prior He et al. [2015]. For classification tasks see App. A.2. As a measure for learning, we consider an observable, which we refer to as *alignment*, given by

$$A_f := \langle f, y \rangle / \langle y, y \rangle, \quad (3)$$

where $\langle g, h \rangle = \int d\mu_x g(x)h(x)$ is the functional inner product, and $d\mu_x$ is some test measure, which, conveniently, does not need to be the measure from which the training set was drawn. We similarly define $\langle g, K, h \rangle = \int d\mu_x d\mu_{x'} g(x)K(x, x')h(x')$ for any kernel K . Alignment represents the extent to which the network learns a function that is proportional to the target. It bounds the test MSE via the Cauchy–Schwarz inequality $\int d\mu_x (f(x) - y(x))^2 \geq \langle y, y \rangle (A_f - 1)^2$. Having $A_f \approx 1$ is thus a necessary condition for successful learning.

3 Alignment and Sample Complexity

We turn to analyze sample complexity via an upper bound on the probability of finding $A_f \geq \alpha$ for $\alpha \approx 1$. We begin with a theoretical bound on the posterior that mainly depends on the chance that a random network, chosen from the prior, produces an alignment of at least α . We denote the prior and posterior alignment probabilities by $\Pr_{p_0}[A_f \geq \alpha]$ and $\Pr_{\pi}[A_f \geq \alpha]$ respectively. Following simple arguments (see App. A and App. A.2 for generalization to classification.), we obtain the following bound on the log posterior²

$$\log(\Pr_{\pi}[A_f \geq \alpha]) < Pk/(2\kappa) + \log(\Pr_{p_0}[A_f \geq \alpha]), \quad (4)$$

where $k = P^{-1} \sum_{\nu=1}^P \mathbb{E}_{p_0}[(f(x_{\nu}) - y(x_{\nu}))^2]$ is the only training-set dependent quantity and is generally of order one. The Bayesian interpretation of successful learning is having $\Pr_{\pi}[A_f \geq \alpha] \approx \mathcal{O}(1)$. Since a random network is unlikely to achieve strong alignment, $\log \Pr_{p_0}[A_f \geq \alpha]$ would typically be highly negative for large α . Therefore, a sufficiently large data term is required to cancel this effect. Explicitly,

$$P \gtrsim -2\kappa \log \Pr_{p_0}[A_f \geq \alpha] / k. \quad (5)$$

Thus, up to the ridge parameter and the $\mathcal{O}(1)$ factor k , depending on the training set, the log probability of prior alignment with the target lower bounds the sample complexity. Here, it is worth noting that the bound becomes tight when overfitting effects are small, which is typically the case for $k/\kappa \sim \mathcal{O}(1)$. Taking $\kappa \rightarrow 0$ encourages overfitting (though often benignly Bartlett et al. [2020]) and trivializes this bound. We conjecture that, in this case, κ should be kept $\mathcal{O}(1)$ based on the effective ridge treatment Canatar et al. [2021b], Cohen et al. [2021], Bartlett et al. [2020]. Establishing this conjecture is outside the scope of this work. From a PAC-Bayesian perspective, an analogous bound would require P to be much larger than the KL-divergence between the prior and posterior (e.g. McAllester [1999]).³. More recently, prior-posterior relations have been studied in the context of complex Boolean functions Mingard et al. [2025].

Following the Chernoff inequality, we can find an upper bound for the probability (and a lower bound for P) via

$$P \geq -2\kappa/k \log \Pr_{p_0}[A_f \geq \alpha] \geq 2\kappa/k E(\alpha), \quad E(\alpha) = -\log \inf_{t>0} e^{-t\alpha} \mathbb{E}_{p_0}[e^{tA_f}]. \quad (6)$$

Where we refer to $E(\alpha)$ as the *energy*. We can thus express the minimal sample size necessary for learning, P_* , through the energy as $P_* \propto E(\alpha)$. In App. B, we provide an asymptotically exact solution for $E(\alpha)$, and compute it explicitly for a two layer network. We also argue and demonstrate that our bound is inherently tied to feature learning. Indeed, a network sampled from the prior that achieves such alignment is a statistical outlier, driven by the emergence of an internal structure which mimics feature learning (see also Fig. 2). Nevertheless, such a direct LDT approach is computationally prohibitive in most cases of interest. We therefore introduce a heuristic LDT-based method for evaluating P_* . This method not only enables predicting the scaling of P_* but also the feature learning effects that lead to successful learning.

In this section, we adopt a variational approach to estimating P_* by comparing different modes of feature learning⁴ under a certain loss (see (10) below). While many approaches predict different

²See also Lavie and Ringel [2025], for a similar data-agnostic bound in the context of lazy learning.

³Following the data-processing-inequality, one can lower-bound the KL-divergence between the full prior and posterior probabilities by the KL-divergence of a coarser probability of an $A_f \geq \alpha$ event in the prior and posterior. The latter KL divergence is given by $-\log \Pr_{p_0}[A_f \geq \alpha]$

⁴Viewed here formally as emergent weight/pre-activation structures enabling the outlier.

feature learning mechanisms Pacelli et al. [2023], Fischer et al. [2024], Meegen and Sompolinsky [2024], Buzaglo et al. [2025], Li and Sompolinsky [2021], Seroussi et al. [2023b], Rubin et al. [2025, 2024], they are often case-dependent, highly detailed, and complex. Thus, we propose a method that abstracts key feature learning mechanisms from these frameworks into distinct, comparable patterns.

4 Variational Analysis

Our next objective is to make the sample complexity bound tractable. This requires estimating the prior probability term, $\Pr_{p_0}[A_f \geq \alpha]$, for alignments $\alpha \approx 1$. As a first step, we simplify this by relating the cumulative distribution function to the probability density denoted by $p_{A_f}(\alpha)$. As shown in App. A.3, for large alignments, we have $E(\alpha) \approx -\log p_{A_f}(\alpha)$. This allows us to re-express P_* in terms of the density: $P_* = -2\kappa \log p_{A_f}(\alpha)/k$. However, computing $p_{A_f}(\alpha)$ directly remains intractable. We therefore turn to a variational approach to estimate it. As explained in the next section, we wish to express the variational probability density in terms of pre-activations h (1). Accordingly, in App. C.1, we follow standard statistical mechanics techniques to express this density as

$$p_{A_f}(\alpha) = \int \mathcal{D}h \mathcal{N}(\alpha | 0, \langle y, \tilde{K}_{L-1}, y \rangle) \prod_{l=1}^{L-1} \prod_{i=1}^{N_l} \mathcal{N}(h_i^l | 0, \tilde{K}_{l-1})$$

Where for each l , the kernels \tilde{K}_{l-1} themselves depend on the preactivations of layer $l-1$, and similarly the fluctuations in α depend on the preactivations of the penultimate layer, given by

$$\tilde{K}_{l>0}(x, x') = \frac{\sigma_{l+1}^2}{N_l} \sum_{i=1}^{N_l} \sigma(h_i^l(x)) \sigma(h_i^l(x')), \quad K_0(x, x') = \frac{\sigma_1^2}{d} x \cdot x' \quad (7)$$

Using statistical mechanics based notation, we define the Hamiltonian $H_{p,\alpha}$ and fluctuating "partition function" Z_{A_f}

$$H_{p,\alpha}(h) = \frac{\alpha^2}{2 \langle y, \tilde{K}_{L-1}, y \rangle} + \frac{1}{2} \sum_{l=1}^{L-1} \sum_{i=1}^{N_l} \langle h_i^l, \tilde{K}_{l-1}^{-1}, h_i^l \rangle, \quad (8)$$

$$\log Z_{A_f}(h) = \log \langle y, \tilde{K}_{L-1}, y \rangle + \sum_{l=1}^{L-1} \text{Tr} \log \tilde{K}_{l-1}.$$

Consequently, $p_{A_f}(\alpha)$ takes the form $p_{A_f}(\alpha) = \int \mathcal{D}h \exp(-H_{p,\alpha}(h) - \log Z_{A_f}(h))$, where the integrand defines an effective measure on the preactivation space for a given α . We next approximate this measure per α by an analytically tractable variational estimate, q . We follow a similar convention here: for any q, α , we define $q_\alpha(h) := Z_{q,\alpha}^{-1} e^{-H_{q,\alpha}(h)}$, requiring that the minimum value of $H_{q,\alpha}(h)$ be zero. For a Gaussian q , this reduces exactly to Eq. 8, with kernels \tilde{K}_{l-1} that are independent of h . The variational computation follows by looking for $q_\alpha(h)$ which minimizes the KL divergence between the measure on h which defines p_{A_f} , and q . The KL divergence can also be used in the estimation of $E(\alpha) := -\log(p_{A_f}(\alpha))$, following the Feynman–Bogoliubov inequality Kuzemsky [2015], Bogolubov and Jr [2009], Huber [1968]. Here we provide a brief description – for

the full derivation see App. C.2. By applying the Feynman–Bogoliubov inequality, we obtain an upper bound on $E(\alpha)$

$$E(\alpha) \approx \min_{q_\alpha} (\mathbb{E}_{h \sim q_\alpha} [\log(Z_{A_f}(h)/Z_{q,\alpha})] + \tilde{E}_q(\alpha)), \quad \tilde{E}_q(\alpha) = \mathbb{E}_{h \sim q_\alpha} [H_{p,\alpha}(h) - H_{q,\alpha}(h)] \quad (9)$$

We argue in App. C.4 that for $\alpha \approx 1$, the log terms are subleading w.r.t. $\tilde{E}_q(\alpha)$. Defining $q_{*,\alpha}$ to be the measure that minimizes $\tilde{E}_q(\alpha)$, we obtain $E(\alpha) \approx \tilde{E}_{q_*}(\alpha)$. Next, we turn to estimating the variational energy $\tilde{E}_q(\alpha)$ Eq. (9) for $\alpha \sim 1$, omitting all α indices for brevity. In App. C.1 we simplify p_{A_f} , and show that the distribution in each layer depends only on the previous through a fluctuating non-linear operator. Next, we assume that this kernel is weakly fluctuating, and replace it with its expectation w.r.t. the variational distribution. This choice approximation aligns with various works on deep non-linear networks, where layer-wise kernels are identified as the relevant and sufficient set of order parameters Rubin et al. [2025], Fischer et al. [2024], Seroussi et al. [2023b], Ringel et al. [2025]. We further take a decoupled Gaussian variational ansatz so that $q(h) = \prod_{l=1}^{L-1} \prod_{i=1}^{N_l} q_{l,i}(h_i^l)$ where $q_{l,i}$ is Gaussian with mean $\mu_{l,i}$ and variance $Q_{l,i}$. As shown in App. C.3, the variational energy estimate is then given by

$$\tilde{E}_q \propto \sum_{l=1}^{L-1} \sum_{i=1}^{N_l} \underbrace{\left(\mathbb{E}_{h \sim \mathcal{N}(\mu_{l,i}, Q_{l,i})} [\langle h, K_{l-1}^{-1} - Q_{l,i}^{-1}, h \rangle] + \langle \mu_{l,i}, Q_{l,i}^{-1}, \mu_{l,i} \rangle \right)}_{=: \Delta_{l,i}} + \underbrace{\langle y, K_{L-1}, y \rangle^{-1}}_{=: a_y}, \quad (10)$$

where we define $K_l = \mathbb{E}_{h \sim q}[\tilde{K}_l]$. Here, the $\Delta_{l,i}$ terms arise from the difference between the approximated kernel and the actual one, and the a_y term results from enforcing an alignment $\alpha \approx 1$. Requiring that q minimize \tilde{E}_q and $\alpha \approx 1$, we estimate $\tilde{E}_q \propto E(\alpha \approx 1) \propto P_*$. Another interpretation of $\Delta_{l,i}$, discussed in App. D, is the excess weight due to feature learning. This viewpoint is useful for feature learning patterns involving circuits, as the latter have a sharp imprint in weight-space. The above kernel viewpoint is, however, more general and can be used both for circuits and for more distributed learning patterns.

5 Heuristics for Manual Computation of Variational approximation

5.1 Feature Learning Patterns

While the above variational approach allows a variety of candidate q ’s, we focus on the previously mentioned set of feature-learning scenarios that have been extensively studied in the literature. Although this subset may appear restrictive, by varying behaviors among layers and between different neurons of the same layer, it already captures a wide range of phenomena. We then need to compare the variational energy (\tilde{E}_q), as detailed in Sec. 4, for such combinations and select the minimizer. The optimal pattern is an indication of the feature learning that emerges in the network to enable strong alignment, as motivated in App. A.3. Concretely, per layer and neuron pre-activation ($h_i^l(x)$), we allow one of the following choices, as illustrated in Fig.

(1) Gaussian Process (GP). Here, $q_{l,i}$ is a Gaussian process (GP) so that $h_{l,i} \sim \mathcal{N}(0, K_{l-1})$ with K_{l-1} defined as the expectation of the kernel defined in (7). This choice defines the “base

model” of feature learning. For FCNs,⁵ it implies that the network propagates feature structure forward without altering latent features (see Sec. 5.2). When all layers and neurons follow this distribution, the network reduces to the neural network GP (NNGP) Neal [1996], where no feature learning occurs. Introducing any of the patterns below in a subset of neurons enables feature learning to emerge.

(2) Gaussian Feature Learning (GFL). In this scenario, pre-activations remain Gaussian with zero mean, but the covariance is modified relative to the GP scenario (1): the kernel of the previous layer is amplified by a factor D in the direction of a specific feature (e.g. an eigenfunction of K_{l-1}) Φ_*^l .⁶ Thus, here too, the distribution is a GP but with a different covariance $Q_{l,i}$ given by

$$Q_{l,i}(x, x') = K_{l-1}(x, x') + D\langle\Phi_*^l, K_{l-1}, \Phi_*^l\rangle \Phi_*^l(x)\Phi_*^l(x'). \quad (11)$$

(3) Specialization. In this scenario, a given neuron specializes to a particular feature Φ_*^l with proportionality constant $\mu_{l,i}$. This pattern corresponds to a Gaussian distribution which is sharply peaked around a non-zero mean $\mu_{l,i}\Phi_*^l$.⁷ Explicitly, we define the distribution of the specialized neuron as

$$q_{l,i}(\langle h_i^l, \Phi_*^l \rangle) = \delta[\langle h_i^l, \Phi_*^l \rangle - \mu_{l,i}], \quad q_{l,i}(\langle h_i^l, \Phi_\perp^l \rangle) = \mathcal{N}(0, \langle \phi_\perp^l, K_{l-1}, \Phi_\perp^l \rangle). \quad (12)$$

5.2 Layer-wise Feature Propagation

Since the variational energy of each layer depends on the kernel of the previous layer, an important element in our heuristic is understanding how the choice of pattern in a given layer affects the kernel and its spectrum in the subsequent layer. To this end, we define feature learning as any deviation from the baseline GP pattern (see Sec. 5.1), such as introducing a non-zero mean to the distribution (i.e., specialization) or altering its covariance structure (i.e., GFL). In our framework, a ”feature” refers either to the mean $\mu_{l,i}$ of $q_{l,i}$ or to an eigenfunction of its covariance operator $Q_{l,i}(x, x')$.

We now outline several key claims concerning how features typically propagate between layers in FCNs. In this context, we consider a data measure that is i.i.d. Gaussian with zero mean and variance 1, not because it approximates the data well, but rather because it provides an unbiased baseline (see also Lavie and Ringel [2025]) for measuring function overlaps. Depending on the input, other choices can also be considered (e.g. permutation-symmetric measures over discrete tokens Lavie et al. [2024]). The following claims with their justifications should be understood as heuristic principles or rationalizations of empirically observed phenomena. Proving them in general or augmenting for different architectures is left for future work. For further details and empirical results, see App. C.5.

Claim (i): Neuron specialization creates a spectral spike. Assume that M neurons in layer l specialize on a single feature $\Phi_*^l(x)$, the subsequent kernel K_l develops a new, dominant spectral feature corresponding to $\sigma(\Phi_*^l(x))$. The corresponding RKHS norm of this feature is amplified, scaling as $\mathcal{O}(N_l/M)$. **Justification:** When M neurons specialize, the next layer’s kernel is approximately $K_l(x, x') = A(x, x') + \frac{M}{N_l}\sigma(\Phi_*^l(x))\sigma(\Phi_*^l(x'))$, where A is the contribution from

⁵For CNNs, even in the lazy regime, deeper kernels have different input scope and hence do generate new structure.

⁶One may also consider generalizations to several features.

⁷Taking equilibrated networks and increasing the amount of data, specialization was shown in Rubin et al. [2024] to emerge as a first-order phase transition where the average of preactivations suddenly shifts to $\mu_{l,i}$. This behavior was further associated with Grokking, suggesting a potential specialization-grokking link.

the non-specialized neurons. Treating the specialization term as a rank-1 update, the Sherman-Morrison formula shows that its RKHS norm becomes $(R_A^{-1} + M/N)^{-1}$, where R_A is the RKHS norm of A , which satisfies $R_A^{-1} \ll M/N$ in typical high-dimensional settings.

Claim (ii): Amplified features in the pre-activation kernel create amplified higher-order features in the post-activation kernel. If a feature $\Phi_*^l(x)$ in kernel K_l has its eigenvalue enhanced by a factor D (i.e., $\lambda_* \rightarrow \lambda_* D$), then the corresponding m -th order power of this feature $(\Phi_*^l)^m(x)$ will have the bulk of its spectral decomposition, under the downstream kernel, shifted up by D^m , with similar effect on the inverse RKHS norm. **Justification:** A Taylor expansion of K_{l+1} in terms of the eigenfunctions of K_l shows that the term corresponding to $(\Phi_*^l)^m(x)$ will have a coefficient scaling with $(\lambda_* D)^m$. We argue that this term is difficult to span using other terms in this expansion, allowing us to treat it as a spectral spike and analyze it similarly to Claim (i). A numerical demonstration of this effect is shown in Fig. 5.

Claim (iii): Lazy layers preserve the relative scale of features from the previous layer. In the absence of feature learning, a properly normalized lazy layer approximately preserves the eigenspectrum of the previous kernel. If a feature $\Phi_*^l(x)$ has an eigenvalue λ_* with respect to the pre-activation kernel given by K_{l-1} , its effective eigenvalue with respect to the post-activation kernel K_l will also be proportional to λ_* . **Justification:** Follows from Claim (ii) taking $D = 1$.

Propagation rules for FCNs

- (1) **Specialization:** Layer l specialized M neurons on Φ_*^l . For any feature Φ satisfying $\langle \sigma(\Phi_*^l), \Phi \rangle \neq 0$, we approximate $\langle \Phi, K_l^{-1}, \Phi \rangle \propto \left[\sum_{i \text{ sp.}} \frac{\mu_{i,l}^2}{N_l} \right]^{-1}$, where we sum over all specializing neurons.
- (2) **GFL:** Layer l amplified fluctuation along Φ_*^l by D so that $\langle \Phi_*^l, K_l^{-1}, \Phi_*^l \rangle = (D\lambda_*)^{-1}$, where λ_* is the GP value of the inner product. Then for any m we have $\langle (\Phi_*^l)^m, K_l^{-1}, (\Phi_*^l)^m \rangle \propto (D\lambda_*)^{-m}$.

6 Concrete Examples

We now apply the heuristic principles of Sec. 4, 5.1, 5.2 to derive sample complexity bounds in a few examples. In App. E.1, we benchmark our method on two-layer FCNs and simple CNNs with non-overlapping patches. There we reproduce both the sample complexity exponent $P_* = d^{3/4}$ identified for CNNs in Ringel et al. [2025] and further predict that $P_* = d$ for two-layer FCNs studying a Hermite-3 target as well as the scaling of the number of specializing neurons with width (see Fig. 2). The latter is also a setting for which the prior's upper bound can be computed directly from $E(\alpha)$ using Large Deviation Theory, leading to a good match with experiment (Fig. 2 panel (a)).

Going to what we believe is beyond the current analytical state of the art, in App. E.3, we predict a $P_* = \sqrt{L}$, where L is the context length, of a softmax attention layer learning a cubic target (see Fig. 3). Another such instance, discussed in detail below, is that of a 3-layer non-linear network learning a non-linear target. In App. A.2 we show that this approach can be extended to classification tasks as well, on non-Gaussian data. In App. E.2 we apply our heuristics to a concrete setting, of a two-layer ReLU network trained on a parity task. We find there as well are able to predict the emergent feature pattern, which qualitatively differs from erf networks. Rather

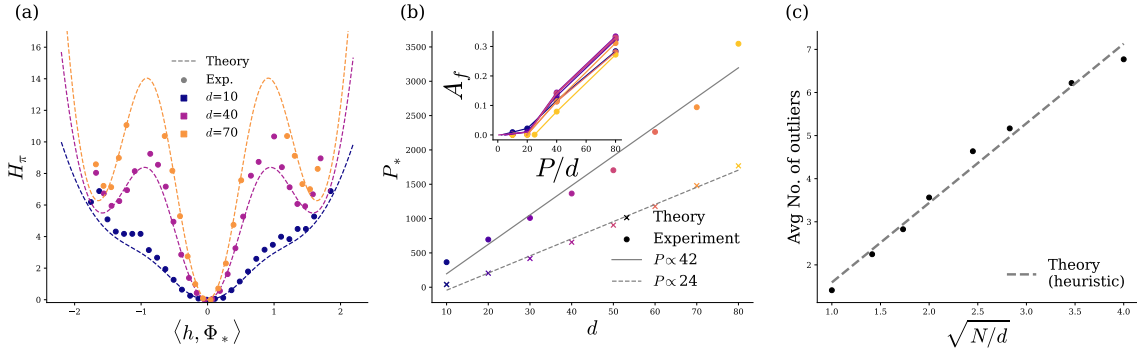


Figure 2: Numerical and experimental results for a two-layer erf network trained on the normalized third Hermite polynomial ($m = 3$). In panel (a) we compare the experimental results and exact theoretical predictions (computed utilizing LDT, see App. B) for the distribution of the alignment of the hidden layer pre-activation with the linear feature. Here we follow the same notation as in (8), so that H_π is the negative log posterior of the preactivations up to an additive constant that enforces zero minimum. We also find the pre-activation distribution corresponds to $q(h)$ for $q \sim M\text{-}Sp$, as predicted by our heuristic approach. Panel (b) compares theoretical and experimental predictions for P_* , defined as alignment $\alpha > 0.1$ (inset shows alignment as a function of sample size). Both theoretical and experimental results agree on $P_* \propto d$. In (c), we increase N and keep P and d fixed, and plot the number of specialized neurons in the hidden layer. In agreement with our heuristic predictions, the number of neurons increases linearly with $\sqrt{N/d}$.

than identifying the scaling number of specializing neurons, we find that there is a finite number of neurons and we are able to predict their scale.

6.1 The Three-layer Network

Here we consider a three-layer FCNs given by

$$f(x) = \sum_{i=1}^{N_2} a_i \sigma \left(\sum_{j=1}^{N_1} w_{ij}^{(2)} \sigma(w_j^{(1)} \cdot x) \right), \quad (13)$$

where $x \in \mathbb{R}^d$ is drawn from $\mathcal{N}(0, I_d)$. We train these networks on a polynomial target of degree m given by $y(x) = He_m(w_* \cdot x)$ where He_m is the m -th probabilist Hermite polynomial, which is the standard polynomial choice under our choice of data measure, and $w_* \in \mathbb{R}^S$ is some normalized vector. The networks are trained via Langevin dynamics Welling and Teh [2011b], with ridge parameter κ , quadratic weight decay, and standard scaling. For an extension to mean-field scaling, see App. E.1.1.

As a starting point for our analysis, consider the simplest pattern ($q = \text{GP-GP}$), having two GP/lazy layers where taking an l 'th layer to be lazy means $Q_{l,i} = K_{l-1}$ and $\mu_{l,i} = 0$. Following the choice of pattern, our goal is to estimate the scaling of \tilde{E}_q . Examining Eq. (10), we find that the $\Delta_{l=1,2,i}$ contributions all cancel by our above choice of Q 's and μ 's. The only non-zero contribution thus comes from the final layer and is given by the inverse of $\langle y, K_2, y \rangle$. Because of lazy learning,

$K_2(x, x')$ is a standard dot product FCN kernel which can be expanded as $\sum_{n=1}^{\infty} a_n(x \cdot x'/d)^n$, with $a_n = O(1)$ w.r.t. $N_{1,2}, d, P$. It can then be shown that $\langle y, K_2, y \rangle = O(d^{-m})$. Leading to $\tilde{E}_{GP-GP} = a_y \propto d^m$.

Next, we consider a feature learning pattern wherein the first layer is GP distributed but the second has feature learning ($q = \text{GP-Sp.}$). Specifically, for the $l = 1$ layer, we take $Q_{1,i} = K_0; \mu_{1,i} = 0$ thereby nullifying again $\Delta_{1,0}$ in Eq. 10 for \tilde{E}_q . For the second layer, we assume M_2 specializing neurons (e.g. $i = 1..M_2$) which fluctuate around the linear feature $(w_* \cdot x)$, while others are lazy, namely $Q_{2,i > M_2} = K_1, \mu_{2,i > M_2} = 0$ and $Q_{2,i=1..M_2} = K_1, \mu_{2,i=1..M_2}(x) = (w_* \cdot x)$. Examining $\sum_{i=1}^{N_2} \Delta_{2,i}$ in Eq. 10, we get zero contributions from $\Delta_{2,i > M_2} = 0$ and $M_2 \langle (w_* \cdot x), K_1^{-1}, (w_* \cdot x) \rangle$ from $i = 1..M_2$. As K_1 is again a simple FCN dot product kernel with no feature learning effects, normalized linear functions such as $w_* \cdot x$ have an $O(d)$ RKHS norm. We thus obtain an overall contribution to \tilde{E}_q from the $l = 2$ layer equal to $M_2 d$. Finally, we need to estimate $a_y = \langle y | K_2 | y \rangle^{-1}$. Note that K_2 is not a standard FCN kernel anymore, since Q_2 , which contains target information, is used in its definition as the expectation of the kernel appearing in (Eq. 7). According to our feature propagation rule (i), with $\Phi_* = (w_* \cdot x)$, we have $a_y = N_2/M_2$. Given M_2 , we thus obtain a variational energy of $M_2 d + N_2/M_2$. We next need to minimize over free parameters, namely M_2 leading to $M_2 = \sqrt{N_2/d}$ and finally $\tilde{E}_{GP-Sp.} = \sqrt{N_2 d}$. Provided N_2 scales less than d^{2m-1} ($N_2 = o(d^{2m-1})$), this pattern is favorable to $\text{GP} - \text{GP}$.

Finally, we consider what turns out to be the favorable pattern consisting of M_1 neurons specializing on $(w_* \cdot x)$ in the first layer and all neurons in the second layer specializing $He_m(w_* \cdot x)$ in the second layer, with a small proportionality constant $\mu_{2,i} = \pm \sqrt{\beta/N_2}$ ($q = \text{Sp.-Mag.}$). We refer to the second-layer pattern as magnetization. Following straightforward adaptation previous argument to this pattern, the variational energy for this pattern as well as others, for $m = 3$, can be found in Table 1.

Feature Pattern	Δ_1	Δ_2	a_y	Minimizing Parameters	\tilde{E}
GP-GP	0	0	d^3	—	d^3
GP-Sp.	0	$M_2 d$	$\frac{N_2}{M_2}$	$M_2 = \sqrt{\frac{N_2}{d}}$	$\sqrt{N_2 d}$
Sp.-Mag.	$M_1 d$	$\frac{N_1}{M_1} \beta$	$\frac{N_2}{\beta}$	$\beta = \left(\frac{N_2^2}{N_1 d} \right)^{1/3}, \quad M_1 = \left(\frac{N_2 N_1}{d^2} \right)^{1/3}$	$(N_1 N_2 d)^{1/3}$

Table 1: Variational energy \tilde{E} for different choices of feature-learning patterns in a three-layer FCN trained on $y(x) = He_3(w_* \cdot x)$. The patterns shown here are (first/second layer): GP-GP, GP-Specialization, and Specialization-Magnetization. For each pattern, the components of the variational energy (Δ_1, Δ_2, a_y) together with the corresponding minimizing parameters are shown. We comment that the GP-GP pattern is favorable only for $d > N_2^5$, and otherwise feature learning will emerge.

In the non-GP q patterns, we obtain the same scaling of \tilde{E}_q in the proportional limit ($N_1 \propto N_2 \propto d$), namely, $P_*/\kappa \propto d$. This observation is validated experimentally in Fig. 3, where the transition to non-zero alignment becomes sharper in the thermodynamic limit ($d \rightarrow \infty$). However, the mechanism by which this scaling is realized changes. In the specialization-magnetization pattern the sample complexity scales with $N_1^{1/3}$, therefore, it increases with N_1 . However, under the GP-specialization pattern, sample complexity does not scale with N_1 , making this pattern preferable.

This prediction is in line with experimental results (see Figs. 8 and 3 panel (c)) where increasing N_1 causes the described change in feature learning patterns. Our prediction also accurately determines the scaling of the number of specializing neurons with N_1 .

6.2 Softmax Attention

Here, we consider an attention block of the form

$$f(X) = \frac{1}{\sqrt{L}} \sum_{h=1}^H \sum_{a,b=1}^L @_{ab;h}(X)(w_h \cdot x^b) \quad @_{ab;h}(X) = e^{[x^a]^\top A_h x^b} \left(\sum_{c=1}^L e^{[x^a]^\top A_h x^c} \right)^{-1}, \quad (14)$$

where $X \in \mathbb{R}^{L \times d}$, $A \in \mathbb{R}^{d \times d}$, and $x^a \in \mathbb{R}^d$ is the a -th row of X , and $w_h \in \mathbb{R}^d$. Our prior on network weights is $\prod_{h=1}^H \mathcal{N}(0, I_{d^2}/d^2; A_h) \mathcal{N}(0, I_d/(dH); w_h)$. The only dependence on the context length L arises from the pre-factor $1/\sqrt{L}$, which ensures that for $X_i^a \sim \mathcal{N}(0, 1)$, we have $f(X) = \mathcal{O}(1)$. The target function is given by $y(X) = \sum_{a,b} \frac{1}{\sqrt{L(L-1)}} x_1^a x_2^b x_3^b$, also normalized to be $\mathcal{O}(1)$. Following our approach, we propose two patterns for this architecture: GP (or lazy learning) and specialization (where we take $A_h \sim \mathcal{N}(\mu \sigma_x \otimes I_{(d-2)}, I_{d^2})$ for $\sigma_x = [1, 0; 0, 1]$ and optimize over μ). As detailed in E.3, the variational energy scales as Ld^3 for the GP pattern and as $\sqrt{HLD^3}$ for the specialization pattern, the latter thus being favorable for H scaling less than $\sqrt{Ld^3}$. As shown in Fig. 3, this scaling of P with L and d indeed matches the dependence of the sample complexity on L .

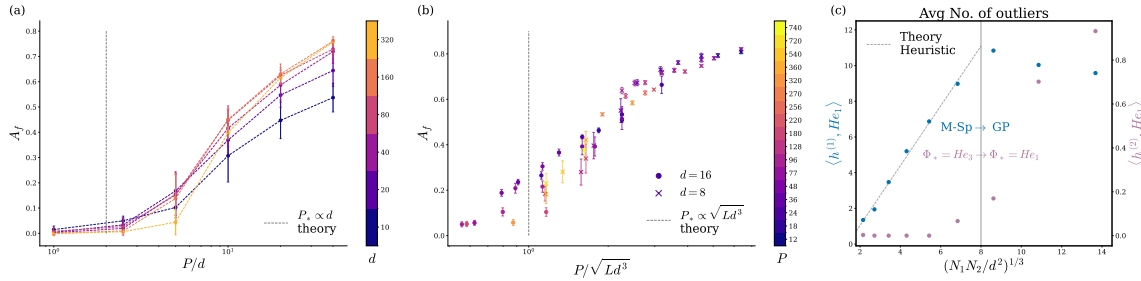


Figure 3: **Sample complexity:** Heuristic predictions accurately capture sample complexity in both three-layer erf FCNs and softmax attention heads, as well as feature learning scaling. Panels (a),(b) both track how the network alignment changes as a function of the ratio between the sample size, P , and the predicted sample complexity- P/d for the FCN in panel (a), and $P/\sqrt{Ld^3}$ for the attention head in panel (b). In both cases, we observe that the alignment collapses onto a single curve, confirming the predicted sample complexity, where good alignment is achieved. See Fig. 9 for comparison to MSE. See E.3 and F.1 for experimental details. **Feature learning patterns:** Panel (c) tracks the number of linearly specialized neurons, in both the first (blue) and second (purple) layers as the first-layer width N_1 varies (with fixed P, d and N_2). The number of first-layer specializing neurons initially follows the predicted $(N_1/d)^{(1/3)}$ scaling before the predicted transition occurs, where second-layer neurons begin to specialize on the linear feature rather than the cubic one, and the first layer neurons approach the GP distribution.

7 Discussion

This paper presents a novel methodology for analyzing the scaling behavior of sample complexity, through which we can also understand how distinct learning mechanisms emerge. Its strength lies in abstracting away from fine-grained details to isolate the core principles at play. We hope such a strategy would remove barriers and expedite connections between mechanistic interpretability and first-principles scientific approaches.

Limitations. Notwithstanding, several avenues for improvement remain. In particular, quantifying feature propagation in more general CNNs and transformers, and addressing multi-feature interaction effects as those appearing in the context of superposition Elhage et al. [2022]. It would also be desirable to extend our heuristic to dynamics of learning, potentially drawing insights from previous work relating equilibrium and dynamical phenomena Power et al. [2022], Rubin et al. [2024], Bahri et al. [2024], Nam et al. [2024]. Since Bayesian convergence times can be slow, correctly predicting the emergence of feature learning in early stages of training may also be highly advantageous. Finally, in some cases, such as under mean-field scaling or vanishing ridge, overfitting effects can emerge, leaving our lower bound vacuous. Extending our approach to patterns that align only on the training set and incorporating effective ridge ideas Canatar et al. [2021a] is thus desirable.

Acknowledgments N.R. and Z.R. acknowledge support from the the Israeli Science Foundation (ISF) Grant No. 374/23.

References

Laurence Aitchison. Why bigger is not always better: on finite and infinite neural networks. *arXiv preprint arXiv:1910.08013*, 2019.

Laurence Aitchison. Deep kernel machines and fast solvers for deep kernel machines. *arXiv preprint arXiv:2108.13097*, 2021.

S Ariosto, R Pacelli, M Pastore, F Ginelli, M Gherardi, and P Rotondo. Statistical mechanics of deep learning beyond the infinite-width limit. *arXiv preprint arXiv:2209.04882*, 2022.

Luca Arnaboldi, Ludovic Stephan, Florent Krzakala, and Bruno Loureiro. From high-dimensional & mean-field dynamics to dimensionless ODEs: A unifying approach to SGD in two-layers networks. *arXiv e-prints*, art. arXiv:2302.05882, February 2023. doi: 10.48550/arXiv.2302.05882.

Yasaman Bahri, Ethan Dyer, Jared Kaplan, Jaehoon Lee, and Utkarsh Sharma. Explaining neural scaling laws. *Proceedings of the National Academy of Sciences*, 121(27):e2311878121, 2024. doi: 10.1073/pnas.2311878121. URL <https://www.pnas.org/doi/abs/10.1073/pnas.2311878121>.

Peter L. Bartlett, Philip M. Long, Gábor Lugosi, and Alexander Tsigler. Benign overfitting in linear regression. *Proceedings of the National Academy of Sciences*, 117(48):30063–30070, December 2020. ISSN 0027-8424, 1091-6490. doi: 10.1073/pnas.1907378117. URL <https://www.pnas.org/doi/full/10.1073/pnas.1907378117>.

Leonard Bereska and Efstratios Gavves. Mechanistic interpretability for ai safety – a review, 2024. URL <https://arxiv.org/abs/2404.14082>.

Alberto Bietti, Joan Bruna, Clayton Sanford, and Min Jae Song. Learning single-index models with shallow neural networks. *Advances in Neural Information Processing Systems*, 35:9768–9783, 2022.

N. N. Bogolubov and Nickolai N. Bogolubov Jr. *Introduction To Quantum Statistical Mechanics (2nd Edition)*. World Scientific Publishing Company, December 2009. ISBN 978-981-310-095-4. Google-Books-ID: t2JIDQAAQBAJ.

Blake Bordelon and Cengiz Pehlevan. Self-consistent dynamical field theory of kernel evolution in wide neural networks. *Advances in Neural Information Processing Systems*, 35:32240–32256, 2022.

Blake Bordelon, Lorenzo Noci, Mufan Li, Boris Hanin, and Cengiz Pehlevan. Depthwise hyperparameter transfer in residual networks: Dynamics and scaling limit. In *NeurIPS 2023 Workshop on Mathematics of Modern Machine Learning*, 2023. URL <https://openreview.net/forum?id=6pfCFDPhy6>.

Gon Buzaglo, Itamar Harel, Mor Shpigel Nacson, Alon Brutzkus, Nathan Srebro, and Daniel Soudry. How Uniform Random Weights Induce Non-uniform Bias: Typical Interpolating Neural Networks Generalize with Narrow Teachers, February 2025. URL <http://arxiv.org/abs/2402.06323> [cs].

Abdulkadir Canatar, Blake Bordelon, and Cengiz Pehlevan. Spectral bias and task-model alignment explain generalization in kernel regression and infinitely wide neural networks. *Nature Communications*, 12(1), May 2021a. ISSN 2041-1723. doi: 10.1038/s41467-021-23103-1. URL <http://dx.doi.org/10.1038/s41467-021-23103-1>.

Abdulkadir Canatar, Blake Bordelon, and Cengiz Pehlevan. Spectral bias and task-model alignment explain generalization in kernel regression and infinitely wide neural networks. *Nature Communications*, 12(1):2914, May 2021b. ISSN 2041-1723. doi: 10.1038/s41467-021-23103-1. URL <https://www.nature.com/articles/s41467-021-23103-1>.

J.L. Cardy. *Scaling and Renormalization in Statistical Physics*. Cambridge lecture notes in physics. Cambridge University Press, 1996. ISBN 9787506238229. URL <https://books.google.co.il/books?id=g5hfPgAACAAJ>.

Youngmin Cho and Lawrence K Saul. Kernel Methods for Deep Learning. *NIPS*, pages 1–9, 2009.

Omry Cohen, Or Malka, and Zohar Ringel. Learning Curves for Deep Neural Networks: A Gaussian Field Theory Perspective. *Physical Review Research*, 3(2):023034, April 2021. ISSN 2643-1564. doi: 10.1103/PhysRevResearch.3.023034. URL <http://arxiv.org/abs/1906.05301>. arXiv:1906.05301 [cs].

Hugo Cui. High-dimensional learning of narrow neural networks, 2025. URL <https://arxiv.org/abs/2409.13904>.

Bernard Derrida. Random-energy model: Limit of a family of disordered models. *Physical Review Letters*, 45(2):79–82, 1980. doi: 10.1103/PhysRevLett.45.79.

Nelson Elhage, Tristan Hume, Catherine Olsson, Nicholas Schiefer, Tom Henighan, Shauna Kravec, Zac Hatfield-Dodds, Robert Lasenby, Dawn Drain, Carol Chen, Roger Grosse, Sam McCandlish, Jared Kaplan, Dario Amodei, Martin Wattenberg, and Christopher Olah. Toy models of superposition. *Transformer Circuits Thread*, 2022. https://transformer-circuits.pub/2022/toy_model/index.html.

Kirsten Fischer, Javed Lindner, David Dahmen, Zohar Ringel, Michael Krämer, and Moritz Helias. Critical feature learning in deep neural networks, May 2024. URL <http://arxiv.org/abs/2405.10761>. arXiv:2405.10761 [cond-mat].

Florentin Guth, Brice Ménard, Gaspar Rochette, and Stéphane Mallat. A rainbow in deep network black boxes. *Journal of Machine Learning Research*, 25(350):1–59, 2024. URL <http://jmlr.org/papers/v25/23-1573.html>.

Kaiming He, Xiangyu Zhang, Shaoqing Ren, and Jian Sun. Delving Deep into Rectifiers: Surpassing Human-Level Performance on ImageNet Classification. *arXiv e-prints*, art. arXiv:1502.01852, February 2015. doi: 10.48550/arXiv.1502.01852.

Joel Hestness, Sharan Narang, Newsha Ardalani, Gregory Diamos, Heewoo Jun, Hassan Kianinejad, Md. Mostofa Ali Patwary, Yang Yang, and Yanqi Zhou. Deep learning scaling is predictable, empirically, 2017. URL <https://arxiv.org/abs/1712.00409>.

Albrecht Huber. Variational Principles in Quantum Statistical Mechanics. In R. C. Clark and G. H. Derrick, editors, *Mathematical Methods in Solid State and Superfluid Theory*, pages 364–392. Springer US, Boston, MA, 1968. ISBN 978-1-4899-6214-0 978-1-4899-6435-9. doi: 10.1007/978-1-4899-6435-9_14. URL http://link.springer.com/10.1007/978-1-4899-6435-9_14.

Jared Kaplan, Sam McCandlish, Tom Henighan, Tom B. Brown, Benjamin Chess, Rewon Child, Scott Gray, Alec Radford, Jeffrey Wu, and Dario Amodei. Scaling laws for neural language models. 2020.

A. L. Kuzemsky. Variational Principle of Bogoliubov and Generalized Mean Fields in Many-Particle Interacting Systems. *International Journal of Modern Physics B*, 29(18):1530010, July 2015. ISSN 0217-9792, 1793-6578. doi: 10.1142/S0217979215300108. URL <http://arxiv.org/abs/1507.00563> [cond-mat].

Itay Lavie and Zohar Ringel. Demystifying Spectral Bias on Real-World Data, February 2025. URL <http://arxiv.org/abs/2406.02663>. arXiv:2406.02663 [stat].

Itay Lavie, Guy Gur-Ari, and Zohar Ringel. Towards Understanding Inductive Bias in Transformers: A View From Infinity, May 2024. URL <http://arxiv.org/abs/2402.05173>. arXiv:2402.05173 [cs].

Qianyi Li and Haim Sompolinsky. Statistical mechanics of deep linear neural networks: The back-propagating kernel renormalization. *Phys. Rev. X*, 11:031059, Sep 2021. doi: 10.1103/PhysRevX.11.031059. URL <https://link.aps.org/doi/10.1103/PhysRevX.11.031059>.

Stephan Mandt, Matthew D Hoffman, and David M Blei. Stochastic gradient descent as approximate bayesian inference. *arXiv preprint arXiv:1704.04289*, 2017.

David A. McAllester. Pac-bayesian model averaging. In *Proceedings of the Twelfth Annual Conference on Computational Learning Theory*, COLT '99, page 164–170, New York, NY, USA, 1999. Association for Computing Machinery. ISBN 1581131674. doi: 10.1145/307400.307435. URL <https://doi.org/10.1145/307400.307435>.

Alexander van Meegen and Haim Sompolinsky. Coding schemes in neural networks learning classification tasks, June 2024. URL <http://arxiv.org/abs/2406.16689>. arXiv:2406.16689 [cs].

Chris Mingard, Guillermo Valle-Pérez, Joar Skalse, and Ard A Louis. Is sgd a bayesian sampler? well, almost. *arXiv preprint arXiv:2006.15191*, 2020.

Chris Mingard, Lukas Seier, Niclas Göring, Andrei-Vlad Badelita, Charles London, and Ard Louis. Characterising the inductive biases of neural networks on boolean data, 2025. URL <https://arxiv.org/abs/2505.24060>.

Yoonsoo Nam, Nayara Fonseca, Seok Hyeong Lee, Chris Mingard, and Ard A. Louis. An exactly solvable model for emergence and scaling laws in the multitask sparse parity problem, 2024. URL <https://arxiv.org/abs/2404.17563>.

Gadi Naveh, Oded Ben David, Haim Sompolinsky, and Zohar Ringel. Predicting the outputs of finite deep neural networks trained with noisy gradients. *Physical Review E*, 104(6), Dec 2021. ISSN 2470-0053. doi: 10.1103/physreve.104.064301. URL <http://dx.doi.org/10.1103/PhysRevE.104.064301>.

Radford M. Neal. *Bayesian Learning for Neural Networks*, volume 118 of *Lecture Notes in Statistics*. Springer New York, New York, NY, 1996. ISBN 978-0-387-94724-2 978-1-4612-0745-0. doi: 10.1007/978-1-4612-0745-0. URL <http://link.springer.com/10.1007/978-1-4612-0745-0>.

R. Pacelli, S. Ariosto, M. Pastore, F. Ginelli, M. Gherardi, and P. Rotondo. A statistical mechanics framework for Bayesian deep neural networks beyond the infinite-width limit. *Nature Machine Intelligence*, 5(12):1497–1507, December 2023. ISSN 2522-5839. doi: 10.1038/s42256-023-00767-6. URL <https://www.nature.com/articles/s42256-023-00767-6>.

Alethea Power, Yuri Burda, Harri Edwards, Igor Babuschkin, and Vedant Misra. Grokking: Generalization beyond overfitting on small algorithmic datasets. *arXiv preprint arXiv:2201.02177*, 2022.

Zohar Ringel, Noa Rubin, Edo Mor, Moritz Helias, and Inbar Seroussi. Applications of Statistical Field Theory in Deep Learning, April 2025. URL <http://arxiv.org/abs/2502.18553>. arXiv:2502.18553 [stat].

Noa Rubin, Inbar Seroussi, and Zohar Ringel. Grokking as a First Order Phase Transition in Two Layer Networks, May 2024. URL <http://arxiv.org/abs/2310.03789>. arXiv:2310.03789 [stat].

Noa Rubin, Kirsten Fischer, Javed Lindner, David Dahmen, Inbar Seroussi, Zohar Ringel, Michael Krämer, and Moritz Helias. From Kernels to Features: A Multi-Scale Adaptive Theory of Feature Learning, 2025. URL <https://arxiv.org/abs/2502.03210>. Version Number: 2.

David Saad and Sara A. Solla. Exact solution for on-line learning in multilayer neural networks. *Phys. Rev. Lett.*, 74:4337–4340, May 1995. doi: 10.1103/PhysRevLett.74.4337. URL <https://link.aps.org/doi/10.1103/PhysRevLett.74.4337>.

Inbar Seroussi, Gadi Naveh, and Zohar Ringel. Separation of scales and a thermodynamic description of feature learning in some cnns. *Nature Communications*, 14(1):908, Feb 2023a. ISSN 2041-1723. doi: 10.1038/s41467-023-36361-y. URL <https://doi.org/10.1038/s41467-023-36361-y>.

Inbar Seroussi, Gadi Naveh, and Zohar Ringel. Separation of scales and a thermodynamic description of feature learning in some CNNs. *Nature Communications*, 14(1):908, February 2023b. ISSN 2041-1723. doi: 10.1038/s41467-023-36361-y. URL <https://www.nature.com/articles/s41467-023-36361-y>.

Max Welling and Yee Whye Teh. Bayesian learning via stochastic gradient langevin dynamics. In *Proceedings of the 28th International Conference on International Conference on Machine Learning*, ICML’11, pages 681–688, USA, 2011a. Omnipress. ISBN 978-1-4503-0619-5. URL <http://dl.acm.org/citation.cfm?id=3104482.3104568>.

Max Welling and Yee Whye Teh. Bayesian Learning via Stochastic Gradient Langevin Dynamics. In *Proceedings of the 28th International Conference on International Conference on Machine Learning*, ICML’11, page 681–688, Madison, WI, USA, 2011b. Omnipress. ISBN 9781450306195.

Andrew Gordon Wilson. The Case for Bayesian Deep Learning, 2020. URL <https://arxiv.org/abs/2001.10995>. Version Number: 1.

Andrew Gordon Wilson and Pavel Izmailov. Bayesian Deep Learning and a Probabilistic Perspective of Generalization, 2020. URL <https://arxiv.org/abs/2002.08791>. Version Number: 4.

Greg Yang, Edward J. Hu, Igor Babuschkin, Szymon Sidor, Xiaodong Liu, David Farhi, Nick Ryder, Jakub Pachocki, Weizhu Chen, and Jianfeng Gao. Tensor programs v: Tuning large neural networks via zero-shot hyperparameter transfer, 2022. URL <https://arxiv.org/abs/2203.03466>.

Mitigating the Curse of Detail: Supplementary material

A Upper Bounds on Posterior Alignment

In this appendix, we derive bounds on the posterior probability of alignment between the network output and the target function. Our goal is to identify the scaling of the minimal sample size P_* as a function of the input dimension, d , required for learning. The derivation proceeds by first relating posterior probabilities of trained network outputs to the prior. While the prior probability is estimated heuristically in C, we provide here a rigorous method for computing this bound using large-deviation techniques.

A.1 The Posterior Bound

Let f_Θ be the output of a network with a given set of trainable weights Θ . Following standard derivations Neal [1996], the posterior distribution of possible outputs of such a network, conditioned on training on data $X \in \mathbb{R}^{P \times d}$ with respect to target $y : \mathbb{R}^d \rightarrow \mathbb{R}$ (which we assume is normalized for simplicity), with MSE loss and ridge parameter κ , is given by

$$\pi(f) = \frac{1}{Z} \exp\left(-\frac{|f(X) - y(X)|^2}{2\kappa}\right) p_0(f), \quad (15)$$

where f and y are applied row-wise to X , $|\cdot|$ is the L_2 norm on the training set, $p_0(f)$ is the prior distribution, defined by

$$p_0(f) = \int d\Theta p(\Theta) \delta[f - f_\Theta], \quad (16)$$

$p(\Theta)$ is the prior weight distribution, and $\delta[f - f_\Theta]$ is the functional delta function Ringel et al. [2025]. We are interested in an upper bound on the posterior probability of achieving alignment $\geq \alpha$, where we define alignment by $A_f := \langle f, y \rangle = \int d\mu_x f(x)y(x)$. The prior alignment density is given by

$$p_{A_f}(\alpha) = \int d\Theta p(\Theta) \delta(A_{f_\Theta} - \alpha). \quad (17)$$

The prior and posterior probabilities of having alignment over some threshold α are given by $\Pr_{p_0}[A_f \geq \alpha]$ and $\Pr_\pi[A_f \geq \alpha]$, respectively. Since the loss is positive, we have $\Pr_\pi[A_f \geq \alpha] \leq \frac{1}{Z} \Pr_{p_0}[A_f \geq \alpha]$. We proceed by obtaining a lower bound on the partition function Z – the normalization constant of the posterior distribution – given by

$$Z = \mathbb{E}_\Theta \left[e^{-\frac{|f_\Theta(X) - y(X)|^2}{2\kappa}} \right] := \int d\Theta p(\Theta) e^{-\frac{|f_\Theta(X) - y(X)|^2}{2\kappa}}. \quad (18)$$

By Jensen's inequality, we obtain

$$\exp\left(-\frac{\mathbb{E}_\Theta [|f_\Theta(X) - y(X)|^2]}{2\kappa}\right) < Z. \quad (19)$$

Since $f_\Theta \sim \mathcal{N}(0, K)$, for the NNGP kernel K on the training data Cho and Saul [2009], Neal [1996], it follows that $\mathbb{E}_\Theta [|f_\Theta(X) - y(X)|^2] = \text{Tr}(K) + |y(X)|^2$. For our choice of normalization, both

$\text{Tr}(K)$ and $|y(X)|^2$ scale with P . Thus, up to an $\mathcal{O}(1)$ factor $k = P^{-1} \sum_{\nu=1}^P \mathbb{E}_{p_0}[(f(x_\nu) - y(x_\nu))^2]$, we obtain $\mathbb{E}_\Theta [|f_\Theta(X) - y(X)|^2] = Pk$. Substituting this in the posterior upper bound, we obtain

$$\Pr_\pi [A_f \geq \alpha] < \exp \left(\frac{Pk}{2\kappa} \right) \Pr_{p_0} [A_f \geq \alpha], \quad (20)$$

or, equivalently,

$$\log (\Pr_\pi [A_f \geq \alpha]) < Pk / (2\kappa) + \log (\Pr_{p_0} [A_f \geq \alpha]). \quad (21)$$

The r.h.s is thermodynamically large in magnitude, crossing zero only briefly, since large negative values imply a vanishingly small probability of strong alignment, the zero crossing marks the threshold for learning. The minimal sample size necessary for learning is then

$$P_* = -\frac{2\kappa}{k} \log \Pr_{p_0} [A_f \geq \alpha]. \quad (22)$$

We comment that P_* provides an *unlearnability* bound, implying that learning cannot occur with less than P_* . However, we find that P_* is indeed indicative of the start of learning in the cases considered in this work. In certain settings, overfitting effects cause this bound to underestimate the true sample complexity, an effect that requires further study. In the following section, we compute the prior probability of alignment on the RHS using the Chernoff bound and large deviations theory, yielding a better estimation for P_* .

A.2 Classification

In the case of a classification problem, we assume the output $f(x) \in \mathbb{R}^{d_o}$, where d_o denotes the number of categories. The dataset is given in the form of a hot-one encoding $\mathcal{D} = \{(x_\mu, y_\mu)\}_{\mu=1}^P$, where $y_\mu \in \mathbb{R}^{d_o}$ and $(y_\mu)_i = \delta_{c(x_\mu)i}$ for the classification target $c(x)$ taking values in $\{1, \dots, d_o\}$. The cross-entropy loss for this setting is

$$\begin{aligned} \mathcal{L}(f; \mathcal{D}) &= -\sum_{\mu=1}^P \left[\log \left(\frac{e^{-f_{c(x_\mu)}(x_\mu)}}{\sum_{j=1}^{d_o} e^{-f_j(x_\mu)}} \right) \right] \\ &= \sum_{\mu=1}^P \left[f_{c(x_\mu)}(x_\mu) + \log \left(\sum_{j=1}^{d_o} e^{-f_j(x_\mu)} \right) \right] \geq 0 \end{aligned}$$

The derivation

$$\pi(f) = \frac{1}{Z} \exp \left(-\frac{\mathcal{L}(f; \mathcal{D})}{2\kappa} \right) p_0(f), \quad (23)$$

follows that of the MSE loss. We similarly have $\Pr_\pi [A_f \geq \alpha] \leq \frac{1}{Z} \Pr_{p_0} [A_f \geq \alpha]$, since the cross-entropy loss is also positive. The use of Jensen's inequality does not depend on $\mathcal{L}(f; \mathcal{D})$, so we only need to compute $\mathbb{E}_\Theta [\mathcal{L}(f; \mathcal{D})]$.

By Cho and Saul [2009], Neal [1996], we have $f_j \sim \mathcal{GP}(0, K_j)$ for the NNGP kernel K_j . Since we only care about the values of f at \mathcal{D} , we consider $f_j \sim \mathcal{N}(0, K_j)$, $K_j \in \mathbb{R}^{P \times P}$, $(K_j)_{\mu\nu} = K_j(x_\mu, x_\nu)$,

where we overloaded the notation f_j and K_j for simplicity.

$$\begin{aligned}
\mathbb{E}_\Theta [\mathcal{L}(f; \mathcal{D})] &= \mathbb{E}_{f \sim \prod_{j=1}^{d_o} \mathcal{N}(0, K_j)} [\mathcal{L}(f; \mathcal{D})] \\
&= \mathbb{E}_{f \sim \prod_{j=1}^{d_o} \mathcal{N}(0, K_j)} \left[\sum_{\mu=1}^P \left[f_{c(x_\mu)}(x_\mu) + \log \left(\sum_{j=1}^{d_o} e^{-f_j(x_\mu)} \right) \right] \right] \\
&= \sum_{\mu=1}^P \mathbb{E}_{f \sim \prod_{j=1}^{d_o} \mathcal{N}(0, K_j)} \left[f_{c(x_\mu)}(x_\mu) + \log \left(\sum_{j=1}^{d_o} e^{-f_j(x_\mu)} \right) \right]
\end{aligned}$$

Since each summand depends on x_μ alone, we can replace $f \sim \prod_{j=1}^{d_o} \mathcal{N}(0, K_j)$ by $f_\mu \sim \mathcal{N}(0, \Sigma_\mu)$ where $(\Sigma_\mu)_{ij} = \delta_{ij} \sigma_{\mu,j}^2$, $i, j \in \{1, \dots, d_o\}$, $\sigma_{\mu,j}^2 = K_j(x_\mu, x_\mu)$. We will also denote $c_\mu := c(x_\mu)$.

$$\begin{aligned}
\mathbb{E}_\Theta [\mathcal{L}(f; \mathcal{D})] &= \sum_{\mu=1}^P \mathbb{E}_{f_\mu \sim \mathcal{N}(0, \Sigma_\mu)} \left[(f_\mu)_{c_\mu} + \log \left(\sum_{j=1}^{d_o} e^{-(f_\mu)_j} \right) \right] \\
&= \sum_{\mu=1}^P \mathbb{E}_{f_\mu \sim \mathcal{N}(0, \Sigma_\mu)} \left[\log \left(\sum_{j=1}^{d_o} e^{-(f_\mu)_j} \right) \right]
\end{aligned}$$

Let $\psi(f_\mu) := \log \left(\sum_{j=1}^{d_o} e^{-(f_\mu)_j} \right)$, so we end up with

$$\mathbb{E}_\Theta [\mathcal{L}(f; \mathcal{D})] = \sum_{\mu=1}^P \mathbb{E}_{f_\mu \sim \mathcal{N}(0, \Sigma_\mu)} [\psi(f_\mu)]$$

Let us concentrate on a single summand and drop μ from our notation for the moment. By Wick's Theorem, we have

$$\begin{aligned}
\mathbb{E}_{f \sim \mathcal{N}(0, \Sigma)} [\psi(f)] &= e^{\frac{1}{2} \sum_{j=1}^{d_o} \sigma_j^2 \frac{\partial_j^2}{\partial f_j^2}} \psi(f)|_{f=0} \\
&= \psi(0) + \frac{1}{2} \sum_{j=1}^{d_o} \sigma_j^2 \frac{\partial_j^2}{\partial f_j^2} \psi(f)|_{f=0} + \text{H.O.T} \\
&= \log(d_o) + \frac{d_o - 1}{d_o^2} \sum_{j=1}^{d_o} \sigma_j^2 + \text{H.O.T}
\end{aligned}$$

Bringing the sum over datapoints back and assuming $\text{Tr}(K_j)$ scales as P , we have

$$\mathbb{E}_{f \sim \prod_{j=1}^{d_o} \mathcal{N}(0, K_j)} [\mathcal{L}(f; \mathcal{D})] = P \log(d_o) + \underbrace{\frac{1}{d_o} \sum_{j=1}^{d_o} \text{Tr}(K_j)}_{\mathcal{O}(P)} + \mathcal{O}\left(\frac{P}{d_o}\right)$$

where the subleading correction $\mathcal{O}(P/d_o)$ comes from an $\mathcal{O}(1/d_o)$ contribution of the $2n$ -th derivative for $n \geq 2$ combined with summation over d_o classes and P stems from the summation over

datapoints. Thus, for a classification task, we obtain

$$\Pr_{\pi} [A_f \geq \alpha] < \exp \left(\frac{P \log(d_o)}{2\kappa} \right) \Pr_{p_0} [A_f \geq \alpha], \quad (24)$$

Consequently, Eq. 22 applies with the necessary adjustment, replacing k with $\log(d_o)$.

Our use of Wick's Theorem to compute the disorder-averaged log-partition function over classes is closely related to the annealed and quenched free-energy calculations that appear in the statistical-physics literature on disordered systems. In that language, for fixed data \mathcal{D} and random parameters Θ , the quantity $-\mathcal{L}(f_\Theta; \mathcal{D})$ plays the role of a random energy, and $-\mathbb{E}_\Theta[\mathcal{L}(f_\Theta; \mathcal{D})]$ is the quenched free energy of a disordered system with d_o states. Our leading term $P \log(d_o)$ is then the purely entropic contribution coming from d_o equiprobable states per datapoint, in direct analogy with the $N \log(2)$ term in Derrida's random-energy model Derrida [1980] for a system with 2^N configurations. In the spin-glass literature, one often replaces the quenched average $\mathbb{E}[\log(Z)]$ by the annealed approximation $\log \mathbb{E}[Z]$, which follows from Jensen's inequality for log and is accurate in the replica-symmetric/high-temperature phase. Our calculation stays on the quenched side and is elementary (Gaussian integrals plus Wick's theorem), but the resulting scaling structure – an entropic $\log(d_o)$ term with subleading corrections controlled by the covariance of the random energies – is entirely consistent with this broader statistical-mechanics viewpoint.

A.3 The Chernoff Upper Bound

We refine the posterior bound using the Chernoff inequality. This allows us to estimate the probability of achieving alignment $\geq \alpha$ under the prior distribution, leading to an explicit expression for the corresponding sample complexity (22). From the Chernoff bound, we get

$$\Pr_{p_0} [A_f \geq \alpha] \leq \inf_{t>0} e^{-t\alpha} \mathbb{E}_\Theta [e^{tA_f}] =: e^{-E(\alpha)}. \quad (25)$$

Substituting in (22), we obtain a new estimate

$$P_* = \frac{2\kappa}{k} E(\alpha). \quad (26)$$

Our aim is to better estimate $E(\alpha)$. Following standard complex analysis derivation, we have

$$\begin{aligned} -\log(\Pr_{p_0} [A_f \geq \alpha]) &\geq E(\alpha) := -\log(\inf_{t>0} \mathbb{E}_\Theta [\exp(t(A_{f_\Theta} - \alpha))]) \\ &= -\log(\text{ext} \mathbb{E}_\Theta [\exp(it(A_{f_\Theta} - \alpha))]), \end{aligned} \quad (27)$$

where ext denotes the extremum with respect to a complex t . Since we are in the rare event regime, we can apply a saddle point approximation to the Fourier transform of $p_{A_f}(\alpha)$

$$p_{A_f}(\alpha) = \frac{1}{2\pi} \int dt \mathbb{E}_\Theta [\exp(it(A_{f_\Theta} - \alpha))] \approx \text{ext}_{t \in \mathbb{C}} \mathbb{E}_\Theta [\exp(it(A_{f_\Theta} - \alpha))]. \quad (28)$$

Thus, (25) can be reduced to

$$-\log \Pr_{p_0} [A_f \geq \alpha] \geq -\log p_{A_f}(\alpha) \approx E(\alpha). \quad (29)$$

This definition of the upper bound allows for further simplifications.

B An Explicit Equation for the LDT Bound in Fully Connected Networks

To make our LDT analysis concrete, we now focus on FCNs. This can be trivially adapted to other architectures, however, such as CNNs and transformers. Here, we provide an explicit expression for the minimal t_* in Eq. 25. The resulting formula involves high-dimensional, non-Gaussian integrals and is therefore highly computationally intensive. We also work out the two-layer case explicitly, where we show that the solution can be reduced to one-dimensional integrals.

B.1 Setup

We begin by specifying the architecture and notation used throughout this section. Focusing on FCNs of depth $L > 1$, we define the forward pass and parameterization explicitly:

$$\begin{aligned} f(x) &= \sum_{i=1}^{N_{L-1}} w_i^L \sigma(h_i^{L-1}(x)) \\ h_i^l(x) &= \sum_{j=1}^{N_{l-1}} W_{ij}^l \sigma(h_j^{l-1}(x)) \quad l = 2, \dots, L-1, \quad i = 1, \dots, N_l \\ h_i^1(x) &= [W^1 x]_i, \quad i = 1, \dots, N_1 \end{aligned}$$

We train the network using Langevin dynamics Welling and Teh [2011a] with MSE loss on a target function y . The quadratic weight decay for each layer l is set to $\kappa N_{l-1}/\sigma_l^2$ where κ is the ridge parameter (corresponding to the Langevin dynamics temperature, T Ringel et al. [2025]) and $N_0 = d$ is the input dimension. We define $\sigma_L^2, \kappa \sim \mathcal{O}(1/\chi)$, where we refer to χ as the mean-field (MF) scale. This choice of weight decay results in a Gaussian prior distribution for the weights given by $W_{i,j}^l \sim \mathcal{N}(0, \sigma_l^2/N_{l-1})$ for $i = 1, \dots, N_l$, $j = 1, \dots, N_{l-1}$.

B.2 Derivation

In the following, we will derive an explicit equation for t_* that minimizes the upper bound for $\Pr_{p_0}[A_f \geq \alpha]$ in (25). We will use Θ^l to denote the weights up to (and including) layer l , in particular, $\Theta^L \equiv \Theta$. Utilizing this notation, we can separate the readout weights,

$$\begin{aligned} \mathbb{E}_\Theta \left[e^{t(A_f - \alpha)} \right] &\propto \\ e^{-t\alpha} \int \prod_{i=1}^{N_{L-1}} dw_i^L d\Theta^{L-1} p(\Theta^{L-1}) \exp \left(-\frac{N_{L-1}}{2\sigma_L^2} (w_i^L)^2 + t \sum_{i=1}^{N_L} w_i^L \langle \sigma(h_i^{L-1}(x)), y(x) \rangle \right). \end{aligned} \quad (30)$$

We integrate out the weights of the final layer to get

$$\mathbb{E}_\Theta \left[e^{t(A_f - \alpha)} \right] \propto e^{-t\alpha} \int d\Theta^{L-1} p(\Theta^{L-1}) \exp \left(\underbrace{\frac{\sigma_L^2}{2N_{L-1}} t^2 \sum_{i=1}^{N_{L-1}} \langle \sigma(h_i^{L-1}(x)), y(x) \rangle^2}_{A_\sigma^2(\Theta^{L-1})} \right). \quad (31)$$

If α is such that it is smaller than the upper bound of A_f , which occurs naturally for unbounded f as in our case where the readout weights are unbounded, then $t_* \in (0, \infty)$. Thus, t_* is determined by minimizing with respect to t , and we obtain

$$\begin{aligned} 0 &= \frac{\partial \mathbb{E}_\Theta [e^{t(A_f - \alpha)}]}{\partial t} \Big|_{t=t_*} \\ &= -\alpha e^{-t\alpha} \int d\Theta^{L-1} p(\Theta^{L-1}) \exp \left(\frac{\sigma_L^2}{2N_{L-1}} \sum_{i=1}^{N_{L-1}} t^2 A_{\sigma,i}^2(\Theta^{L-1}) \right) \\ &\quad + \sum_{i=1}^{N_{L-1}} \frac{\sigma_L^2}{N_{L-1}} t e^{-t\alpha} \int d\Theta^{L-1} p(\Theta^{L-1}) A_{\sigma,i}^2(\Theta^{L-1}) \exp \left(\frac{\sigma_L^2}{2N_{L-1}} \sum_{i=1}^{N_{L-1}} t^2 A_{\sigma,i}^2(\Theta^{L-1}) \right) \Big|_{t=t_*}, \end{aligned}$$

where we have $A_{\sigma,i}^2(\Theta^{L-1}) := \langle \sigma(h_i^{L-1}), y \rangle^2$. Rearranging, we obtain an implicit equation for t_*

$$t_* = \frac{\alpha N_L \int d\Theta^{L-1} p(\Theta^{L-1}) \exp \left(\frac{\sigma_L^2}{2N_{L-1}} t_*^2 A_\sigma^2(\Theta^{L-1}) \right)}{\sigma_L^2 \int d\Theta^{L-1} p(\Theta^{L-1}) A_\sigma^2(\Theta^{L-1}) \exp \left(\frac{\sigma_L^2}{2N_{L-1}} t_*^2 A_\sigma^2(\Theta^{L-1}) \right)}, \quad (32)$$

which takes a simpler form, using the notation $\mathbb{E}_{\Theta^{L-1}}[(\dots)] = \int d\Theta^{L-1} p(\Theta^{L-1})(\dots)$,

$$t_* = \frac{\alpha N_{L-1} \mathbb{E}_{\Theta^{L-1}} \left[\exp \left(\frac{\sigma_L^2}{2N_{L-1}} t_*^2 A_\sigma^2(\Theta^{L-1}) \right) \right]}{\sigma_L^2 \mathbb{E}_{\Theta^{L-1}} \left[A_\sigma^2(\Theta^{L-1}) \exp \left(\frac{\sigma_L^2}{2N_{L-1}} t_*^2 A_\sigma^2(\Theta^{L-1}) \right) \right]}. \quad (33)$$

B.3 Exact LDT Saddle-point Computation for a Two-layer Network

To illustrate the general framework in a more tractable setting, we analyze a simple two-layer FCN. In this case, the derivation simplifies substantially, allowing us to obtain explicit analytical expressions assuming $x \sim \mathcal{N}(0, I_d)$. Concretely, consider the setting

$$y(x) = \hat{H}e_3(w_* \cdot x), \quad \sigma = \text{erf}, \quad L = 2$$

where $w_* \in \mathbb{R}^d$ is some normalized vector, and $\hat{H}e_3$ is the normalized third probabilist Hermite polynomial. Since this is a simple two-layer network, we need only consider the weights of the hidden layer themselves, and not the pre-activations. For brevity, we also drop layer indexing ($W \equiv W^1 = \Theta^1$, $N \equiv N_1$, $d = N_0$), since there is only one relevant layer, and take $\sigma_1^2, \sigma_2^2 = 1$, in particular, we assume standard scaling. Following (33), we obtain

$$t_* = \frac{\alpha N \mathbb{E}_W \left[\exp \left(\frac{1}{2N} t_*^2 A_\sigma^2(W) \right) \right]}{\mathbb{E}_W \left[A_\sigma^2(W) \exp \left(\frac{1}{2N} t_*^2 A_\sigma^2(W) \right) \right]}$$

where $A_\sigma^2(W) = \sum_{i=1}^N \langle \sigma(w_i \cdot x), y(x) \rangle^2$, using $w_i \in \mathbb{R}^d$ for the i -th row of W . Since W is i.i.d. in the different neuron indices, the above equation becomes

$$t_* = \frac{\alpha \int d^d w \exp \left(-\frac{d}{2} |w|^2 + \frac{1}{2N} t_*^2 A_\sigma^2(w) \right)}{\int d^d w A_\sigma^2(w) \exp \left(-\frac{d}{2} |w|^2 + \frac{1}{2N} t_*^2 A_\sigma^2(w) \right)} \quad (34)$$

where $A_\sigma^2(w) = \langle \sigma(w \cdot x), y(x) \rangle^2$, $w \in \mathbb{R}^d$, $w \in \mathcal{N}(0, \frac{1}{d} I_d)$. This inner product can be calculated explicitly. For a general (normalized) probabilist Hermite polynomial, using the Hermite Rodrigues formula together with high-order integration by parts (as a generalization of Stein's identity) produces

$$\begin{aligned} \mathbb{E}_{x \sim \mathcal{N}(0, I_d)} [\hat{H} e_n(w_*^\top x) \sigma(w^\top x)] &= \frac{(w_*^\top w)^n}{n!} \mathbb{E}_{x \sim \mathcal{N}(0, I_d)} [\sigma^{(n)}(w^\top x)] \\ &= \frac{(w_*^\top w)^n}{n!} \mathbb{E}_{t \sim \mathcal{N}(0, |w|^2)} [\sigma^{(n)}(t)] \end{aligned}$$

assuming $|w_*| = 1$, where $\sigma^{(n)}$ stands for the the n -th derivative of σ . From here on, we simply use erf's third derivative giving us straight-forward Gaussian integrals to calculate that produce

$$\langle \text{erf}(w \cdot x), y(x) \rangle^2 = \frac{4}{9\pi} \left(\frac{w \cdot w_*}{\sqrt{1 + 2|w|^2}} \right)^6 \quad (35)$$

Next, assuming that all components of w perpendicular to w_* are weakly fluctuating, we can approximate

$$\frac{w \cdot w_*}{\sqrt{1 + 2|w|^2}} \approx \frac{w \cdot w_*}{\sqrt{1 + 2(w_* \cdot w)^2 + 2 \sum_{\perp} \mathbb{E}_{w \cdot w_{\perp}} [(w \cdot w_{\perp})^2]}} \approx \frac{w \cdot w_*}{\sqrt{3 + 2(w_* \cdot w)^2}},$$

where \sum_{\perp} denotes a sum over an orthonormal basis in weight space, w_{\perp} , which are orthogonal to w_* . Using $\mathbb{E}_{w \sim \mathcal{N}(0, \frac{1}{d} I_d)} [g(w \cdot w_*)] = \mathbb{E}_{\beta \sim \mathcal{N}(0, \frac{1}{d})} [g(\beta)]$ for $\beta = w \cdot w_*$ with a unit vector w_* , and for any function g , we can apply the above approximation to (34) to get

$$t_* \approx \frac{9\alpha\pi \mathbb{E}_{\beta \sim \mathcal{N}(0, \frac{1}{d})} \left[\exp \left(\frac{2}{9\pi N} t_*^2 \left(\frac{\beta}{\sqrt{3+2\beta^2}} \right)^6 \right) \right]}{4 \mathbb{E}_{\beta \sim \mathcal{N}(0, \frac{1}{d})} \left[\left(\frac{\beta}{\sqrt{3+2\beta^2}} \right)^6 \exp \left(\frac{2}{9\pi N} t_*^2 \left(\frac{\beta}{\sqrt{3+2\beta^2}} \right)^6 \right) \right]}$$

If we then denote

$$S(\beta; t_*) = \beta^2 - \frac{4t_*^2}{9\pi N d} \left(\frac{\beta}{\sqrt{3+2\beta^2}} \right)^6, \quad (36)$$

we end up with

$$t_* \approx \frac{9\alpha\pi}{4} \cdot \frac{\int d\beta \exp(-\frac{d}{2} S(\beta; t_*))}{\int d\beta \left(\frac{\beta}{\sqrt{3+2\beta^2}} \right)^6 \exp(-\frac{d}{2} S(\beta; t_*))}, \quad (37)$$

The t_* , which (approximately) solves (37), can then be used to compute the scaling of P_* .

Following the derivation for the upper bound (26), recall that we have

$$P_* \propto -2\kappa \log(e^{-t_* \alpha} \mathbb{E}_{\Theta} [e^{t_* A_f}]) \quad (38)$$

for $k \approx 1$. Following (31), we integrate out the readout weights and utilize our calculation, culminating in (37), to get

$$\begin{aligned} \mathbb{E}_\Theta [e^{t_* A_f}] &= \mathbb{E}_W \left[e^{\frac{1}{2N} \sum_{i=1}^N t_*^2 A_{\sigma,i}^2(W)} \right] \\ &= \prod_{i=1}^N \mathbb{E}_{w_i \sim \mathcal{N}(0, \frac{1}{d} I_d)} \left[e^{\frac{1}{2N} t_*^2 A_\sigma^2(w_i)} \right] \\ &\approx \left[\int d\beta \exp \left(-\frac{d}{2} S(\beta; t_*) \right) \right]^N. \end{aligned} \quad (39)$$

Finally, we arrive at the following expression for sample complexity

$$P_* \propto 2\kappa \left[t_* \alpha - N \log \left(\int d\beta \exp \left(-\frac{d}{2} S(\beta; t_*) \right) \right) \right] \quad (40)$$

To evaluate it, we numerically solve for t_* in (37). The resulting t_* is then used to numerically evaluate the one-dimensional integral in (39) over $\beta = w \cdot w_*$. This produces the sample complexity scale in (40). These computational results are shown in Fig. 2, including predictions both for network output, and weight distribution.

We can gain further insight by interpreting (39) as the partition function (i.e. the normalization factor) of a t_* -dependent, non-Gaussian distribution. This distribution can be understood as representing the required weight configuration for achieving good alignment. While good alignment is improbable under the prior, this new distribution makes it attainable. If this distribution represents the optimal path to alignment within the prior, it is reasonable to infer that it will correspond to the feature learning patterns in the posterior. Indeed, as illustrated in Fig. 2, this is precisely the case, as the posterior weight distribution is closely approximated by the prior alignment distribution we predict. It is this observation that motivates the reasoning in following sections, by guessing various feature learning patterns that result in good alignment in the prior, we can deduce the actual distribution in the posterior. We can compare different guesses, and determine which of the patterns is most likely to emerge.

C Variational Estimate of $E(\alpha)$

As the explicit expression for the energy, $E(\alpha) = -\log p_{A_f}(\alpha)$, is intractable, we turn to computing a variational estimate for this quantity.

C.1 Distribution Analysis in Pre-activation space

We first rewrite p_{A_f} as a distribution on the pre-activations, rather than the network weights. Following A.3, the upper bound for the prior probability is given by

$$\Pr_{p_0} [A_f \geq \alpha] \leq p_{A_f}(\alpha) := \int d\Theta p(\Theta) \delta(A_{f_\Theta} - \alpha). \quad (41)$$

Replacing the delta function with its Fourier representation, $p_{A_f}(\alpha) = \frac{1}{2\pi} \int dt e^{-it\alpha} \hat{p}_{A_f}(t)$, $\hat{p}_{A_f}(t) = \mathbb{E}_\Theta [\exp(itA_f)]$, we obtain

$$p_{A_f}(\alpha) = \frac{1}{2\pi} \int dt \int d\Theta p(\Theta) \exp \left(it \left(\sum_{i=1}^{N_{L-1}} w_i^L \langle y, \sigma(h_i^{L-1}) \rangle - \alpha \right) \right). \quad (42)$$

We can simplify this integral by integrating out the readout weights in the readout layer, as done in (31), which results in

$$p_{A_f}(\alpha) = \frac{1}{2\pi} \int dt \int d\Theta^{L-1} p(\Theta^{L-1}) \exp \left(-\frac{\sigma_L^2}{2N_{L-1}} \sum_{i=1}^{N_{L-1}} t^2 \langle y, \sigma(h_i^{L-1}) \rangle^2 - it\alpha \right) \quad (43)$$

By comparison, in (30) t was real, accounting for the difference in sign. Integrating out t we obtain

$$\begin{aligned} p_{A_f}(\alpha) &= \frac{1}{\sqrt{2\pi}} \int d\Theta^{L-1} p(\Theta^{L-1}) \exp \left(-\frac{\alpha^2}{\frac{2\sigma_L^2}{N_{L-1}} \sum_{i=1}^{N_{L-1}} \langle y, \sigma(h_i^{L-1}) \rangle^2} + \frac{1}{2} \log \frac{1}{\frac{\sigma_L^2}{N_{L-1}} \sum_{i=1}^{N_{L-1}} \langle y, \sigma(h_i^{L-1}) \rangle^2} \right) \\ &= \int d\Theta^{L-1} p(\Theta^{L-1}) \mathcal{N}(\alpha | 0, \kappa_A(h^{L-1}(\Theta^{L-1}))), \end{aligned} \quad (44)$$

where the variance κ_A is given by

$$\kappa_A(h^{L-1}(\Theta^{L-1})) = \frac{\sigma_L^2}{N_{L-1}} \sum_{i=1}^{N_{L-1}} \langle y, \sigma(h_i^{L-1}(\Theta^{L-1})) \rangle^2 \quad (45)$$

and h_i^{L-1} are the final layer's pre-activations, which are themselves determined by the weights of the first $L-1$ layers of the network Θ^{L-1} . We now perform a change of variables by enforcing pre-activations through a delta function and then rewriting it in terms of its Fourier representation. We then obtain

$$\begin{aligned} p_{A_f}(\alpha) &= \int \mathcal{D}h \int dW \int \mathcal{D}m \exp \left(-\sum_{l=1}^{L-1} \sum_{i=1}^{N_l} \sum_{j=1}^{N_{l-1}} \frac{N_{l-1}}{2\sigma_l^2} (W_{ij}^l)^2 \right) \\ &\quad \times \exp \left(i \sum_{l=1}^{L-1} \sum_{i=1}^{N_l} \left[\langle m_i^l, h_i^l \rangle - \left\langle m_i^l, \sum_{j=1}^{N_{l-1}} W_{ij}^l \sigma(h_j^{l-1}) \right\rangle \right] \right) \mathcal{N}(\alpha | 0, \kappa_A(h^{L-1})) \\ &=: \int \mathcal{D}h \tilde{p}(h) \mathcal{N}(\alpha | 0, \kappa_A(h^{L-1})). \end{aligned} \quad (46)$$

Here $\mathcal{D}h$ denotes the path integral over the pre-activation functions h for all layers and neurons, and $\mathcal{D}m$ is the path integral over its Fourier conjugate variables (see [Ringel et al., 2025, Sec. 3.1] for further details). We further specify that the integration measures are normalized to include the appropriate powers of π . When $l=1$ we replace $\sigma(h_j^{l-1})$ with x . We next integrate out the weights

W to obtain

$$\tilde{p}(h) = \int \mathcal{D}m \exp \left(- \sum_{l=1}^{L-1} \sum_{i=1}^{N_l} \sum_{j=1}^{N_{l-1}} \frac{\sigma_l^2}{2N_{l-1}} \langle m_i^l, \sigma(h_j^{l-1}) \rangle^2 + i \sum_{l=1}^{L-1} \sum_{i=1}^{N_l} \langle m_i^l, h_i^l \rangle \right). \quad (47)$$

Finally, we integrate out the auxiliary fields m_i^l to obtain

$$\tilde{p}(h) = \exp \left(- \frac{1}{2} \sum_{l=1}^{L-1} \sum_{i=1}^{N_l} \langle h_i^l, [\tilde{K}_{l-1}]^{-1}, h_i^l \rangle - \frac{1}{2} \text{Tr} \log(\tilde{K}_{l-1}) \right). \quad (48)$$

where the integral operator

$$\tilde{K}_{l-1}(x, x') = \frac{\sigma_l^2}{N_{l-1}} \sum_{j=1}^{N_{l-1}} \sigma(h_j^{l-1}(x)) \sigma(h_j^{l-1}(x'))$$

can be understood as the fluctuating h^{l-1} -dependent kernel and $[\tilde{K}_{l-1}]^{-1}$ is its inverse w.r.t. the measure $d\mu_x$. The above is an exact rewriting of the probability distribution showing that, conditioned on previous layers, each hidden layer has Gaussian pre-activations. Inspired by standard statistical mechanics notation, we define the for \tilde{p} the Hamiltonian $H_{\tilde{p}}(h) = \frac{1}{2} \sum_{l=1}^{L-1} \sum_{i=1}^{N_l} \langle h_i^l, [\tilde{K}_{l-1}]^{-1}, h_i^l \rangle$ and the fluctuating "partition function" $Z_{\tilde{p}}$ such that $\log Z_{\tilde{p}}(h) = \frac{1}{2} \sum_{l=1}^{L-1} \text{Tr} \log(\tilde{K}_{l-1})$. Thus, we can write $\tilde{p}(h) = Z_{\tilde{p}}^{-1}(h) \exp[-H_{\tilde{p}}(h)]$.

C.2 Variational approximation

Turning back to the alignment density p_{A_f} , we can substitute the result from the previous section so that

$$p_{A_f}(\alpha) = \int \mathcal{D}h \exp \left(- \underbrace{\left(H_{\tilde{p}}(h) + \frac{\alpha^2}{2\kappa_A(h^{L-1})} \right)}_{=: -H_{p,\alpha}(h)} - \underbrace{\left(\frac{1}{2} \log \kappa_A(h^{L-1}) + \log Z_{\tilde{p}}(h) \right)}_{=: \log Z_{A_f}(h)} \right) \quad (49)$$

We are interested in computing $E(\alpha)$, which is given by

$$E(\alpha) = -\log p_{A_f}(\alpha) = -\log \int \mathcal{D}h \exp(-H_{p,\alpha}(h)) / Z_{A_f}(h). \quad (50)$$

Since the integral over h is generally intractable, we turn to a variational approximation. The goal of this estimate is to find a simpler, tractable distribution $q_\alpha(h)$ that is in some sense "close" to the true pre-activation density $\exp(-H_{p,\alpha}(h))$ per alpha. We thus define our variational distribution in a similar Hamiltonian

$$q_\alpha(h) = \frac{1}{Z_{q,\alpha}} \exp(-H_{q,\alpha}(h)), \quad (51)$$

where $H_{q,\alpha}$ satisfies $\min_h H_{q,\alpha}(h) = 0$, and $Z_{q,\alpha}$ is the partition function given by $Z_{q,\alpha} = \int \mathcal{D}h \exp(-H_{q,\alpha}(h))$. This choice results in a unique definition of $H_{q,\alpha}$, $Z_{q,\alpha}$ for each distribution q_α . The Feynman-Bogoliubov inequality provides a rigorous definition of closeness between $\exp(-H_{p,\alpha}(h))$ and $q_\alpha(h)$.

This inequality establishes an upper bound on $E(\alpha)$ which depends on the choice of q . The Feynman-Bogoliubov inequality Bogolubov and Jr [2009] states that for any q

$$-\log \left(\int \mathcal{D}h e^{-H_{p,\alpha}(h)} / Z_{A_f}(h) \right) \leq -\log Z_{q,\alpha} + \mathbb{E}_{h \sim q_\alpha} [H_{p,\alpha}(h) - H_{q,\alpha}(h) + \log Z_{A_f}(h)] \quad (52)$$

where $\mathbb{E}_{h \sim q_\alpha} [\cdot]$ is the expectation over h with respect to the distribution q_α . Recalling that $E(\alpha) = -\log p_{A_f}(\alpha)$, this inequality can be used to simplify the bound

$$E(\alpha) \leq \mathbb{E}_{h \sim q_\alpha} [\log(Z_{A_f}(h)/Z_{q,\alpha})] + \mathbb{E}_{h \sim q_\alpha} [H_{p,\alpha}(h) - H_{q,\alpha}(h)] =: \tilde{E}_q(\alpha), \quad (53)$$

We can estimate $E(\alpha)$ by taking q_α which minimizes the upper bound (53). In the following sections we turn to compute the upper bound. Since we consider only $\alpha \approx 1$, we drop α in what follows.

When N_{L-1} is large, κ_A is weakly fluctuating with h^{L-1} , since it is a sum of N_{L-1} random variables. Denoting $\bar{\kappa}_{A_f} = \mathbb{E}_{h \sim \tilde{p}(h)} [\kappa_A(h^{L-1})]$, we have

$$\mathbb{E}_{h \sim q_1} [H_{p,1}(h) - H_{q,1}(h)] \approx \frac{1}{2\bar{\kappa}_A} + \mathbb{E}_{h \sim q} [H_{\tilde{p}}(h) - H_q(h)] \quad (54)$$

to leading order (where $q \equiv q_1$), so that

$$\tilde{E}_q(1) \approx \frac{1}{2\bar{\kappa}_A} + \mathbb{E}_{h \sim q} [H_{\tilde{p}}(h) - H_q(h)] + \mathbb{E}_{h \sim q_\alpha} [\log(Z_{A_f}(h)/Z_{q,\alpha})]. \quad (55)$$

We show in C.4 that the expectation of log term- $\mathbb{E}_{h \sim q_\alpha} [\log(Z_{A_f}(h)/Z_{q,\alpha})]$ is subleading and thus can be neglected. In essence, our variational ansatzes constrain deviations from the GP to a sub-extensive subset of feature directions, such that the resulting corrections do not scale extensively with system size or parameter count. Moreover, since these corrections enter logarithmically, their contribution becomes further subleading. Thus, we have

$$\tilde{E}_q \approx \frac{1}{2\bar{\kappa}_A} + \mathbb{E}_{h \sim q} [H_{\tilde{p}}(h) - H_q(h)] \quad (56)$$

The problem has now been reduced to minimizing \tilde{E}_q with respect to a choice of variational distribution $q(h)$. If we find the optimal q_* that minimizes \tilde{E}_q , we obtain our best estimate for the energy, when $\alpha \approx 1$,

$$E(\alpha \approx 1) \approx \tilde{E}_{q_*}. \quad (57)$$

C.3 Approximate Variational Energy

Our final task is to compute the variational energy $\tilde{E}_q(\alpha)$ given our variational density q . Although we work with Gaussian q 's that are layer-wise and neuron-wise decoupled, this computation is nevertheless challenging due to the presence of h^l , dependence on $[\tilde{K}_l]^{-1}$, and the trace term $\text{Tr} \log(\tilde{K}_l)$. In the spirit of kernel adaptation Ringel et al. [2025], we assume the fluctuations of \tilde{K}_l are sufficiently small and only keep the leading order dependence which dominates $\tilde{E}_q(\alpha)$. In this context, this means replacing the fluctuating kernel \tilde{K}_l with its expectation with respect to q and K_l given by

$$K_l(x, x') = \frac{\sigma_{l+1}^2}{N_l} \sum_{i=1}^{N_l} \mathbb{E}_{h_i^l \sim q(h^l)} [\sigma(h_i^l(x)) \sigma(h_i^l(x'))]. \quad (58)$$

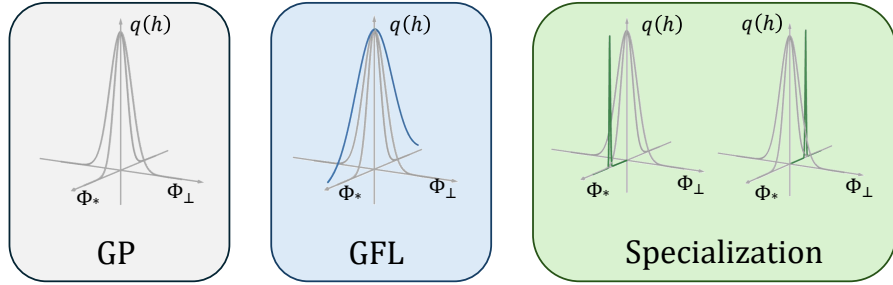


Figure 4: Schematic illustration of different candidate feature learning patterns per neuron.

Following this substitution, we obtain

$$H_{\tilde{p}}(h) = \frac{1}{2} \sum_{l=1}^{L-1} \sum_{i=1}^{N_l} \langle h_i^l, [K_{l-1}]^{-1} h_i^l \rangle \quad (59)$$

and obtain our final tractable expression for the variational energy

$$\tilde{E}_q \approx \frac{1}{2} \langle y, K_{L-1}, y \rangle^{-1} + \frac{1}{2} \mathbb{E}_{h \sim q} \left[\sum_{l=1}^{L-1} \sum_{i=1}^{N_l} \langle h_i^l, K_{l-1}^{-1}, h_i^l \rangle - H_q(h) \right]. \quad (60)$$

Since \tilde{p} is fully decoupled layer and neuron-wise, we similarly take a decoupled variational ansatz so that $q(h) = \prod_{l=1}^{L-1} \prod_{i=1}^{N_l} q_{l,i}(h_i^l)$. Further taking $q_{l,i}$ to be Gaussian with mean $\mu_{l,i}$ and variance $Q_{l,i}$, we obtain

$$\tilde{E}_q = \frac{1}{2} \langle y, K_{L-1}, y \rangle^{-1} + \frac{1}{2} \sum_{l=1}^{L-1} \sum_{i=1}^{N_l} \left\{ \mathbb{E}_{h_i^l \sim q_{l,i}} \left[\langle h_i^l, [K_{l-1}]^{-1} - Q_{l,i}^{-1}, h_i^l \rangle \right] + \langle \mu_{l,i}, Q_{l,i}^{-1}, \mu_{l,i} \rangle \right\} \quad (61)$$

Minimizing the above over all Gaussian q 's results in complex non-linear equations, which we wish to avoid. Instead, we propose minimizing over a small subset of q 's, which we refer to as feature learning patterns. We look to minimize \tilde{E}_q over this finite set and take that to be our variational energy. A summary of all patterns can be found in Fig. 4.

C.3.1 Comparison to Adaptive Kernel Approximation

The similarities and differences between the approach developed here and the adaptive methods discussed in Seroussi et al. [2023a], Ringel et al. [2025] are worth examining. In those works, \tilde{p} is similarly approximated using a mean-field expansion, with two key differences: The chosen mean and the order of expansion around the mean. The fluctuating kernel in these works \tilde{K}_{l-1} is expanded around its *self-consistent mean* $K_{l-1|\tilde{p}}$, rather than the variational expectation introduced here. The self-consistent mean kernel is defined as

$$K_{l>0|\tilde{p}}(x, x') = \frac{\sigma_{l+1}^2}{N_l} \sum_{i=1}^{N_l} \mathbb{E}_{h_i^l \sim \tilde{p}(h)} [\sigma(h_i^l(x)) \sigma(h_i^l(x'))], \quad (62)$$

$$K_{0|\tilde{p}}(x, x') = \frac{\sigma_0^2}{d} x \cdot x'.$$

We define the kernel fluctuations relative to this mean by ΔK_{l-1} , such that $\tilde{K}_{l-1} = K_{l-1|\tilde{p}} + \Delta K_{l-1}$. The adaptive approximations assume that these fluctuations are weak, i.e., $\Delta K_{l-1} \ll K_{l-1|\tilde{p}}$, and retain all terms up to order $\mathcal{O}(\Delta K_{l-1})$, whereas in this work we consider only the zeroth-order term in ΔK_{l-1} . Taking such an approximation in the self-consistent setting would yield the GP distribution, since no feature-learning corrections would be taken into account. In our proposed methodology, because the variational expectation already incorporates feature-learning effects, the simpler expansion can instead be employed.

C.4 Justification for Neglecting the Partition Function Ratio

Here we argue that the logarithmic ratio of partition functions, $\mathbb{E}_{h \sim q_\alpha} [\log(Z_{A_f}(h)/Z_q)]$, is sub-leading relative to the variational energy term \tilde{E}_q (defined in Sec. C.2). We show that this holds for all feature learning patterns considered in this work (Sec. 5.1): GP, GFL, and specialization. Substituting the definition of $Z_{A_f}(h)$ we obtain:

$$\mathbb{E}_{h \sim q_\alpha} [\log Z_{A_f}(h)] = \mathbb{E}_{q_\alpha} \left[\frac{1}{2} \log \kappa_A(h^{L-1}) \right] + \frac{1}{2} \sum_{l=1}^{L-1} \text{Tr} \mathbb{E}_{q_\alpha} [\log(\tilde{K}_{l-1})] \quad (63)$$

We assume that for sufficiently wide networks the fluctuations are weak, so that at least in terms of scales we can approximate

$$\dots \approx \log \mathbb{E}_{q_\alpha} \left[\frac{1}{2} \kappa_A(h^{L-1}) \right] + \frac{1}{2} \sum_{l=1}^{L-1} \text{Tr} \log \mathbb{E}_{q_\alpha} [(\tilde{K}_{l-1})]$$

So that we obtain

$$\mathbb{E}_{h \sim q_\alpha} [\log Z_{A_f}(h)] \approx \frac{1}{2} \sum_{l=1}^{L-1} \text{Tr} \log K_{l-1} + \frac{1}{2} \log \bar{\kappa}_A \quad (64)$$

Recalling that \tilde{E}_q scales linearly with $\bar{\kappa}_A^{-1}$, we can indeed justify neglecting the term $\log \bar{\kappa}_A$ as it is subleading for small $\bar{\kappa}_A$. We will show that the remaining terms can be neglected as well. Using the eigendecomposition of the kernel (58), $K_{l-1}(x, x') = \sum_{k_l} \lambda_{k_l} \Phi_{k_l}(x) \Phi_{k_l}(x')$, the Gaussian integral for a single neuron in layer l evaluates to $\prod_{k_l} \sqrt{2\pi \lambda_{k_l}}$. The logarithm of the full partition function is then

$$\log Z_p = \sum_{l=1}^{L-1} N_l \log \left(\prod_{k_l} \sqrt{2\pi \lambda_{k_l}} \right) =: \sum_{l=1}^{L-1} N_l \log Z_p^l, \quad (65)$$

where we have defined $\log Z_p^l$ as the single-neuron log-partition function under the GP prior. As described in the main text, we consider variational distributions q that fully factorize over layers and neurons. Thus, we can write

$$\log Z_q = \sum_{l=1}^{L-1} \sum_{i=1}^{N_l} \log \int D h_i^l q_{l,i}(h_i^l) =: \sum_{l=1}^{L-1} \sum_{i=1}^{N_l} \log Z_q^{l,i}. \quad (66)$$

Combining these results, the log-ratio of the partition functions decomposes into a sum over per-neuron contributions. We aim to show that, for each neuron, this term is sub-dominant compared

to the corresponding term in the variational energy \tilde{E}_q . Recall (61) that

$$\tilde{E}_q = \frac{1}{2} \langle y, K_L^{-1}, y \rangle + \sum_{l=1}^{L-1} \sum_{i=1}^{N_l} \Delta_{l,i}, \quad (67)$$

where the per-neuron cost $\Delta_{l,i}$ is

$$\Delta_{l,i} := \frac{1}{2} \mathbb{E}_{h \sim q_{l,i}} \left[\langle h, K_{l-1}^{-1} - Q_{l,i}^{-1}, h \rangle + \langle \mu_{l,i}, Q_{l,i}^{-1}, \mu_{l,i} \rangle \right]. \quad (68)$$

Our goal is to show that, for each feature learning pattern, $\Delta_{l,i} + (\log Z_q^{l,i} - \log Z_p^l)$ scales like $\Delta_{l,i}$.

Case-by-Case Analysis

1. **Specialization:** The variational distribution is a delta function

$$q_{l,i}(\langle h_i^l, \Phi_*^l \rangle) = \delta[\langle h_i^l, \Phi_*^l \rangle - \mu_{l,i}], \quad q_{l,i}(\langle h_i^l, \Phi_\perp^l \rangle) = \mathcal{N}(0, \langle \Phi_\perp^l, K_{l-1}, \Phi_\perp^l \rangle). \quad (69)$$

The partition function is given by- $\log Z_q = \sum_{l=1}^{L-1} \sum_{k_l, \Phi_{k_l} \neq \Phi_*} \log \sqrt{2\pi \lambda_{k_l}}$

- **Variational Cost:** The cost term evaluates to $\Delta_{l,i} = \frac{1}{2} \mu_{l,i}^2 \langle \Phi_*, K_{l-1}^{-1}, \Phi_* \rangle$. In typical high-dimensional settings, $\langle \Phi_*, K_{l-1}^{-1}, \Phi_* \rangle$ scales at least with d , so $\Delta_{l,i} = \mathcal{O}(d)$.
- **Partition Function Ratio:** In all but the feature direction, the normalization factor of the variational estimate and the normalization factor of p is equal, and thus cancels out. The only difference is in the feature direction, where we obtain exactly $\log Z_p^l / Z_q^l = -\frac{1}{2} \sum_{i=1}^{N_l} \log(\Delta_{li})$
- **Conclusion:** we thus obtain $Z_p^l / Z_q^l \ll \sum_{i=1}^{N_l} \Delta_{li}$.

2. **Gaussian Feature Learning (GFL):** We have $h \sim \mathcal{N}(0, Q_{l,i})$, where $Q_{l,i}$ shares the same eigenbasis as K_{l-1} , with λ'_{k_l} identical to λ_{k_l} except for the feature Φ_* , where $\lambda'_* = D\lambda_*$.
 - **Variational Cost:** The cost is $\Delta_{l,i} = \frac{1}{2} \text{Tr}(K_{l-1}^{-1} Q_{l,i} - I)$. Since only one eigenvalue differs, this sum reduces to $\Delta_{l,i} = \frac{1}{2}(D-1)$.
 - **Partition Function Ratio:** The log-ratio $\log(Z_q^{l,i} / Z_p^l)$ becomes the log-ratio of the determinants, which is $\frac{1}{2} \log(\det Q_{l,i} / \det K_{l-1}) = \frac{1}{2} \log(D)$.
 - **Conclusion:** For large enhancement factors D , the linear scaling of $\Delta_{l,i} = \mathcal{O}(D)$ dominates the logarithmic scaling of the partition function term, $\mathcal{O}(\log D)$.
3. **GP / Lazy Regime:** This case is equivalent to GFL with $D = 1$.
 - **Conclusion:** Substituting $D = 1$ into the GFL results, we find that both $\Delta_{l,i} = 0$ and the log-partition function term is $\log(1) = 0$. The relationship holds trivially.

C.5 Kernel Feature Propagation

Since the cost of each layer depends on the kernel of the previous layer, an important element of our heuristic is understanding how the choice of pattern in the previous layer affects the kernel and its spectrum. Recall that we denote the pre-activation of the current layer by $h^l(x)$, and of the previous layer by $h^{l-1}(x)$, where $h^{l-1}(x)$ is the width N_{l-1} pre-activation vector of the previous layer. Let h_i^{l-1} be distributed according to some candidate Gaussian distribution $q_i'(h^{l-1})$. We wish to understand how this choice of $q_i'(h^{l-1})$ affects the kernel of the next layer given by

$$K_{l-1}(x, x') = N_{l-1}^{-1} \sum_{i=1}^{N_{l-1}} \mathbb{E}_{h_i^{l-1}(x) \sim q_i} [\sigma(h_i^{l-1}(x)) \sigma(h_i^{l-1}(x'))] =: \sum_{i=1}^{N_{l-1}} K_{l-1,i}(x, x'), \quad (70)$$

where we took $\sigma_l^2 = 1$ for brevity.

Claim (i): Neuron specialization creates a spectral spike. Assume we have an operator of the form $K(x, x') = A(x, x') + c\sigma(\Phi(x))\sigma(\Phi(x'))$ for some constant c . We wish to understand the behavior of the RKHS norm of $\sigma(\Phi)$ with respect to the above operator. Using the Sherman-Morrison formula, we obtain

$$[A + c\sigma(\Phi)\sigma(\Phi)^\top]^{-1} = A^{-1} - \frac{A^{-1}c\sigma(\Phi)\sigma(\Phi)^\top A^{-1}}{1 + c\sigma(\Phi)^\top A^{-1}\sigma(\Phi)}, \quad (71)$$

where vv^\top denotes the outer product. Consequently, the RKHS norm of $\sigma(\Phi)$ with respect to K is given by

$$R_K \equiv \sigma(\Phi)^\top [A + c\sigma(\Phi)\sigma(\Phi)^\top]^{-1} \sigma(\Phi) = R_A - \frac{R_A^2 c}{1 + R_A c} = \frac{R_A}{1 + R_A c} < 1/c \quad (72)$$

where R_A is its RKHS norm w.r.t. A^{-1} . Typically, we would consider large values of R_A . Thus, if we have $cR_A \gg 1$, then $\frac{R_A}{1 + R_A c} \approx c^{-1}$, thereby justifying Claim (i).

Corollary 1. If M of N_l neurons are specialized in a given layer with the rest remaining Gaussian with zero mean, then we can substitute $c = N_l/M$ in the above, and obtain $R_{K_l} = N_l/M$.

Corollary 2. If all neurons are specialized with proportionality constant $\sqrt{\beta}$, then we can substitute $c = \beta$ in the above, and take $A = \epsilon I$ as a regularizer, with $\epsilon \rightarrow 0$, so that $R_A \rightarrow \infty$, and we obtain $R_{K_l} = \beta$.

Claim (ii): Amplified features in the pre-activation kernel create amplified higher-order features in the post-activation kernel. We begin by considering the Gaussian case, where $h_i^l(x) \sim \mathcal{N}(0, Q_l)$ for all i . Since K_l is a dot product kernel for an FCN, we can expand the expectation in (58) to obtain

$$K_l(x, x') = \sum_{a=1}^{\infty} (Q_l(x, x'))^a F_a(x, x'), \quad (73)$$

where $Q_l(x, x')$ is a function of $x \cdot x'$ and $F_a(x, x')$ is a function of $|x|^2$ and $|x'|^2$ derived by expanding the resulting Cho and Saul kernel associated with the activation function σ [Cho and Saul, 2009, §2.3]. We further assume that $Q_l(x, x) \sim \mathcal{O}(1)$ +small fluctuations. This is a reasonable assumption

to make for Gaussian data in high dimensions where $|x|^2 = d \pm \sqrt{d}$. For more general datasets, one should either verify this or apply layer-normalization (as done below for the case of data with power-law covariance spectrum).

Using its Mercer decomposition $Q_l(x, x') = \sum_k \lambda_k \Phi_k(x) \Phi_k(x')$, we have

$$K_l(x, x') \propto \sum_k \lambda_k \Phi_k(x) \Phi_k(x') + \sum_{k_1, k_2} \lambda_{k_1} \lambda_{k_2} \Phi_{k_1}(x) \Phi_{k_2}(x) \Phi_{k_1}(x') \Phi_{k_2}(x') + \dots \quad (74)$$

Next, we ask how enhancing a certain λ_k by a factor D affects the post-activation kernel $K_l(x, x')$. Let λ_{k_*} be some eigenvalue of Q_l corresponding to the eigenfunction $\Phi_*(x)$. It can be potentially adapted via GFL ($\lambda_{k_*} \rightarrow D\lambda_*$ where $D\lambda_* < 1$). Then the $K_{l,i}$ RKHS norm of any feature of the form $\sum_{n=1}^m a_n \Phi_{\lambda_*}^n(x)$ scales like $\mathcal{O}((\lambda_* D)^{-m})$ (assuming $a_m = \mathcal{O}(1)$). Indeed, consider the case $m = 2$ and examine

$$K_l(x, x') \propto \sum_k D_k \lambda_k \Phi_k(x) \Phi_k(x') + \sum_{k_1, k_2} D_{k_1} D_{k_2} \lambda_{k_1} \lambda_{k_2} \Phi_{k_1}(x) \Phi_{k_2}(x) \Phi_{k_1}(x') \Phi_{k_2}(x') + \dots \quad (75)$$

with $D_k = D$ when $\lambda_k = \lambda_*$ and $D_k = 1$ otherwise. The argument proceeds by treating the term $\Phi_*^m(x) \Phi_*^m(x')$ as a rank-1 spike. Substituting K_l for K , $(D\lambda_*)^m$ for c , and Φ^m for $\sigma(\Phi)$ in Claim (i), we obtain $R_{K_l} = (R_A^{-1} + (D\lambda_*)^m)^{-1}$.

The important observation/assumption here is that, for sufficiently large D , $R_A(D\lambda_*)^m \gg 1$ so that $R_{K_l} \approx (D\lambda_*)^{-m}$. This is supported numerically in Figs. 5 and 6. Our analytical reasoning is that the subspace effectively described by the kernel K_l is a negligible portion of the total function space. This is either because the rank of K_l is constrained by network width N_l or its spectrum λ_k exhibits rapid decay. Our analytical rationalization for this is as follows. Either because in a real network, the rank of the kernel K_l is bounded by the network width N_l or because the spectrum λ_k falls down quickly, the effective span of the first term and subsequent terms covers only a negligible fraction of the total function space. In this large function space, it is unlikely that a feature like Φ_*^m is fully contained within this span. If this is the case, its RKHS norm with respect to the base kernel would be large, motivating our observation/assumption.

In Fig. 5, we consider two ReLU-activated layers of an FCN ($L = 4$) and Gaussian i.i.d. data $x \in \mathbb{R}^d, x \sim \mathcal{N}(0, I_d)$. We obtain the empirical NNGP kernel after the first ReLU layer of width $N_1 = 2000$. Diagonalizing the kernel ($K_{l=2}$) on $P = 6000$ sample points $\{x_\nu\}_{\nu=1}^P$, we choose $\Phi_*(x)$ to be the $d/2$ highest eigenvalue. We then look for the best weight vector $a \in \mathbb{R}^{N_1}$ satisfying $\Phi_*(x_\nu) \approx \sum_{i=1}^{N_1} a_i \text{ReLU}(W_i \cdot x_\nu)$, where W_i are the input layer weights used to generate $K_{l=2}$. We draw the rows of $W \in \mathbb{R}^{N_2 \times N_1}$ i.i.d. with $W_i \sim \mathcal{N}(0, I/N_1 + (D-1)\hat{a}\hat{a}^\top/N_1)$, where $\hat{a} = a/\sqrt{a^\top a}$. This mimics the GFL effect. Finally, we compute the kernel empirical kernel following another ReLU layer and compute the RKHS norm of $\Phi_*^2(x)$ with mean removed, omitting eigenvalues which are zero up to machine precision (for $P > N_2$, $P - N_2$ such eigenvalues are to be expected).

In Fig. 6, we perform a similar analysis with the following qualitative changes. The data is chosen to be Gaussian, but non-i.i.d. with a covariance matrix whose k 'th eigenvalue is $k^{-1.1}$. To prevent strong fluctuations of $K_2(x, x)$ (i.e., $Q_2(x, x)$ of Claim (ii)), which are now not suppressed at $d \rightarrow \infty$ we apply layer normalization between the two activated ReLU layers. The top left panel has $d = 250, N_1 = N_2 = 3000$ and uses 4000 datapoints to sample the kernel operator and compute the spectrum used in the RKHS norm. The top right panel is a $\times 4$ scaled-up version of the left panel in terms of N_1, N_2, P and d and shows a longer persistence of $1/D^2$ expected scaling by, roughly, a factor of 2. The bottom panels show the behavior of polynomial activation of the type $\sigma(x) = 1 + x + x^2$, both with (left) and without (right) layer normalization.

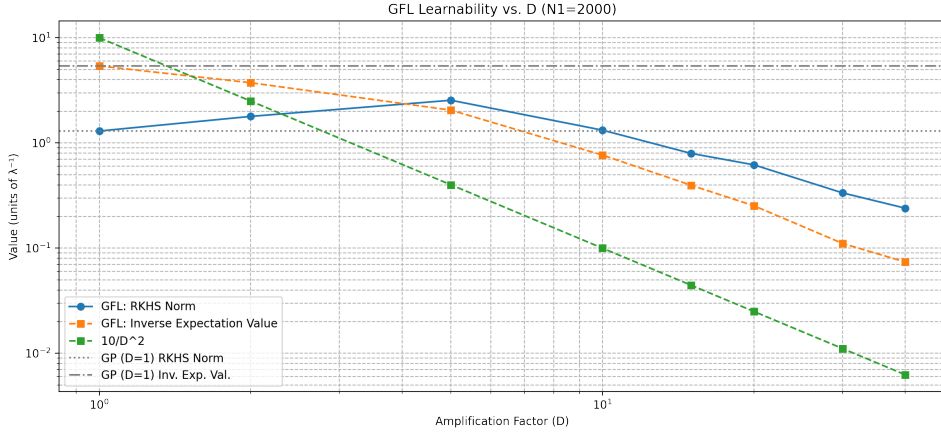


Figure 5: Demonstration GFL feature propagation. We increased the variance of the $d/2$ highest kernel mode $\Phi_*(x)$ of the first hidden layer and then measured $\langle \Phi_* | K_{l=3} | \Phi_* \rangle^{-1}$ and $\langle \Phi_* | [K_{l=3}]^{-1} | \Phi_* \rangle$, where $K_{l=3}$ is the kernel of the subsequent layer. We used ReLU activations, $d = 120$, $N_1 = 2000$, $N_2 = 1000$ and random Gaussian data. This demonstrates the expected D^{-2} decay and the matching between inverse expectation values and the RKHS.

D \tilde{E} and Δ_ℓ in Weight Space

In the main text, we focused on a function space formulation for \tilde{E} , using pre-activations, GP distributions (q) for h^l , and kernel operators. This formulation facilitated the combination of GP-like learning mechanisms and circuit/specialization-based mechanisms. In some cases however, it is more natural to work in weight space (see also Guth et al. [2024] for a weight-space picture analogous to kernel adaptation). One such example is CNNs, for which the distribution of the input layer convolutional-patch-dependent pre-activations, is more readily described in terms of shared input weights. Another example would be an i_0 -th neuron specializing on some j_0 neuron of the upstream layer, which implies a delta-function distribution around $W_{i_0j} \sim \delta_{j,j_0}$. Accordingly, we wish to express $\Delta_{l,i}$ of (68) in weight space. For simplicity, we focus on distributions with zero mean.

To this end, we consider some pre-activation in layer l and write it in terms of layer weights namely, $h_{i_0}^l(x) = \sum_{i=1}^{N_{l-1}} W_{i_0i}^l \sigma(h_i^{l-1}(x))$. For compactness, we henceforth take $W_{i_0i}^l \rightarrow a_i$, $h_{i_0}^l \rightarrow h^l$. We next treat the h_i^{l-1} 's as independent draws from $q_{l-1,i} = q_{l-1}$, consistent with the kernel adaptation approximation, which removes correlations between pre-activation. To avoid operator algebra and work solely with matrices, we consider extremely many (P') draws $\{x_\nu\}_{\nu=1}^{P'}$ from $d\mu_x$ and define the $(l-1)$ -th feature matrix with entries

$$F_{i\nu}^{l-1} := \sigma(h_i^{l-1}(x_\nu)), \quad i = 1, \dots, N_{l-1}, \quad \nu = 1, \dots, P'$$

Note that for large N_{l-1} , $\left[(F^{l-1})^\top F^{l-1} \right]_{\mu\nu} / N_{l-1}$, via the law of large numbers, concentrates to its averages under q and thus approaches $K_{l-1}(x_\mu, x_\nu)$.

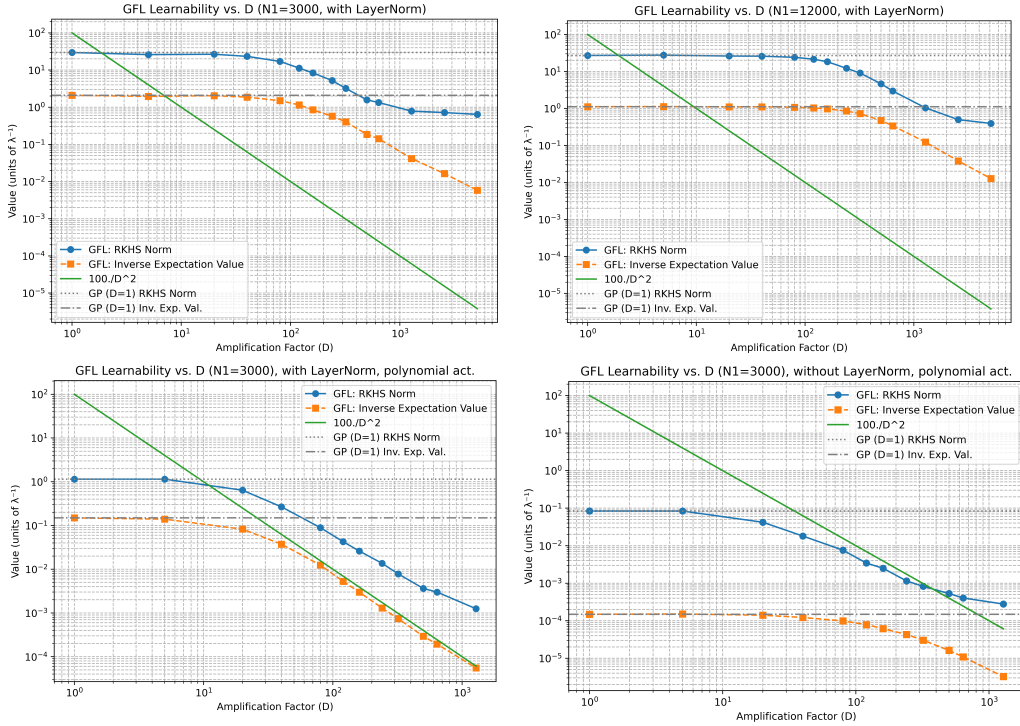


Figure 6: Similar to Fig. 5, only for Gaussian data with power-law covariance matrix with eigenvalues decaying as $k^{-1.1}$. See C.5 for further details.

We next revisit the inter-layer action for $l, l-1$ appearing Eq. (48 given by $\langle h, \tilde{K}^{-1}, h \rangle$ and note that (i) \tilde{K} upon freezing h^{l-1} at some typical value as done above, $\tilde{K} = F^\top F / N_{l-1}$ (ii) the inverse operation is to be understood as a pseudo inverse $((..)^+)$ which removes the contribution of the null space of this (generically) rank- N_{l-1} operator. Following this and the linear relation between h^l and a , we have that

$$\langle h, \tilde{K}_{l-1}^+, h \rangle = a^T F [F^\top F / N_{l-1}]^+ F^\top a = N_{l-1} a^\top a. \quad (76)$$

We thus obtain a reasonable result: The RKHS term, which regulates the pre-activations, is equal to the weight-decay term associated with the a 's that generated that h .

Following this rewriting, one can now repeat our variational approximation in weight space. This results in an analogous formula to Eq. 10 with q_l denoting a Gaussian distribution on a 's ($a \sim \mathcal{N}[\bar{a}^l, \Sigma_l]$), and K_{l-1} (the covariance of the h 's in the action) replaced by I / N_{l-1} (the covariance of a 's in the action).

All in all we obtain the following weight space version of the contribution of the i 'th neuron to \tilde{E}_q , namely

$$\Delta_{l,i} = \mathbb{E}_{a \sim \mathcal{N}(\bar{a}, \Sigma_l)} [a^\top [N_{l-1} I - \Sigma_l^{-1}] a] + \bar{a}^\top \Sigma_l^{-1} \bar{a} \quad (77)$$

E Application of Heuristics for Additional Architectures

E.1 Regression tasks in Two-layer Networks

In the two-layer setting, an exact solution can be obtained, so we begin by comparing our heuristic approach to the exact solution. In this case, we consider both two-layer FCNs as well as CNNs with non-overlapping convolution windows. Together, these are given by

$$f(x) = \sum_{i=1}^{N_w} \sum_{j=1}^N w_{ij}^{(2)} \sigma(w_j^{(1)} \cdot x_i), \quad (78)$$

where $x \in \mathbb{R}^d$ is drawn from $\mathcal{N}(0, I_d)$. We take $d = N_w S$ so that $w_j, x_i \in \mathbb{R}^S$. The vector x_i is given by the $((i-1)S+1)$ -th to iS -th coordinates of x . We train these networks on a polynomial target of degree m given by $y(x) = \sum_{i=1}^{N_w} H e_m(w_* \cdot x_i)$ where $H e_m$ is the m -th probabilist Hermite polynomial, which is the standard polynomial choice under our choice of data measure, and $w_* \in \mathbb{R}^S$ is some normalized vector. The networks are trained via Langevin dynamics Welling and Teh [2011b], with ridge parameter κ , quadratic weight decay, and standard scaling. For an extension to mean-field scaling, see App. E.1.1.

E.1.1 Fully Connected Networks

Standard scaling. We turn to compute \tilde{E}_q for a range of feature learning patterns. For this shallow FCN (and $N_w = 1$), our choice of feature learning patterns amounts to considering distributions in a single layer. We consider the following three scenarios (though more combinations are possible): (1) all neurons are GP distributed, (2) all are GFL distributed with amplification D , and (3) M neurons specialize on a the same feature, while those remaining are GP distributed. As the kernel of the first layer can only express linear features, the only relevant feature to be considered for the GFL and M-specialization patterns is $\Phi_*(x) = w_* \cdot x$. We compute the scale of the optimal variational energy for each pattern:

- (1) **GP:** Here, $\Delta_{1,i} = 0$ since $K_{l-1} = Q_l$. In this baseline setting, learning $m > 1$ is hard since $\langle H e_m | K_2 | H e_m \rangle = \mathcal{O}(d^{-m})$ (see Sec. 5.2). Thus, in total, we have $\tilde{E}_{q \sim \text{GP}} \propto d^m$.
- (2) **GFL:** Following (10), this pattern incurs a cost of $\Delta_{1,i} = D$ per neuron i , resulting in a total cost of ND . The a_y term can be calculated utilizing Claim (ii). This leads to a D^m -factor decrease in the RKHS norm relative to the GP, so that $a_y \propto (d/D)^m$. In total, we find that $\tilde{E}_{q \sim \text{GFL}} \propto ND + (d/D)^m$. Minimizing w.r.t. D , we obtain $D_{\min} = (d^m/N)^{1/(m+1)}$, and, substituting back, we obtain $\tilde{E}_{q \sim \text{GFL}} \propto (Nd)^{\frac{m}{m+1}}$.
- (3) **M-Specialization:** Following 10, this pattern incurs a cost of $\Delta_1 = M \langle \Phi_*, K_0^{-1} \Phi_* \rangle = Md$, where we denote $\Delta_l = \sum_i \Delta_{l,i}$. Utilizing Claim (i), this results in adding a spike with an M/N coefficient along $\sigma(w_* \cdot x)$ in K_1 appearing in a_y . Before this spike, $H e_m(x)$ only had overlaps with the m -th order Taylor expansion of the kernel, leading to a d^{-m} scaling. However, since $\sigma(w_* \cdot x)$ has an $\mathcal{O}(1)$ overlap with $H e_m(x)$, so that $a_y \propto N/M$, we obtain $\tilde{E}_{q \sim \text{M-Sp}} \propto dM + N/M$. Minimizing further over M , the number of specializing neurons leads to $M_{\min} = \sqrt{N/d}$ and therefore $\tilde{E}_{q \sim \text{M-Sp}} \propto \sqrt{dN}$.

Now, we can compare the different feature learning patterns. Taking the most common linear scaling where $N \propto d$, the specialization scenario has the lowest variational energy. Our scaling theory then predicts an $\mathcal{O}(d)$ sample complexity as well as multimodal distribution of w along w_* with $\mathcal{O}(1)$ specializing neurons. Taking $m > 1$ and $N \gg d^5$, lazy learning wins and leads to $\mathcal{O}(d^m)$ complexity. When $m = 1$, GFL and M-specialization are on par for $N \propto d$. These calculations coincide with both experimental and direct LDT results, as demonstrated in Fig. 2 for networks trained on He_3 . In terms of sample complexity, both predictions agree with experiment, with a scaling of $P_* \propto d$, as seen in Fig. 2 (b). Our heuristic approach correctly predicts the scaling of the number of specializing neurons with N , as seen in Fig. 2 (c). Finally, as shown in panel (a), the analytical LDT method recovers the correct pre-activation distribution, which corresponds to $q(h)$ for $q \sim M\text{-Sp}$.

Extension to Mean-field Scaling Here we extend the results presented in the main text to the case of mean-field scaling. We note that the results presented for standard scaling can change when introducing mean-field parametrization, amounting here to enhancing the alignment factor by a $\chi = \mathcal{O}(N)$ factor. The GP pattern then results in a much worse energy $\tilde{E}_{GP} = Nd^3$. Revisiting the GFL pattern, we now find $\tilde{E}_{GFL} = ND + N(d/D)^m$ leading to $D \propto d^{1/(m+1)}$ and $\tilde{E}_{GFL,optimal} \propto Nd^{m/(m+1)}$. For specialization, we obtain $\tilde{E}_{sp} = dM + N^2/M$, leading to $M \propto N/\sqrt{d}$ and $\tilde{E}_{sp,optimal} \propto \sqrt{d}N$. Taking $N \propto d$, the specialization scenario again wins over for $m > 1$, with a sub-extensive ($\mathcal{O}(\sqrt{d})$) number of specializing neurons. Unlike with standard-parametrization, we see that even when taking $N \rightarrow \infty$, we remain in the rich regime. However, at least in this Bayesian finite-ridge setting, sample complexity is better with standard parametrization.

E.1.2 CNNs with Non-overlapping Patches.

Our approach can be extended to the CNN in (13) with $N_w > 1$. In this case, it is better to focus on the covariance of w_i , namely, $\Sigma = N^{-1} \sum_{i=1}^N w_i w_i^T$, than on the covariance of pre-activations on each path. One can then show that the cost becomes $\Delta_1 = \mathbb{E}_{q_w} w^\top [\Sigma^{-1} - I_S/S] w$.

- (1) **GP:** In this scenario, the output kernel is given by $K_{2,CNN}(x, x') = N_w^{-1} \sum_{i=1}^{N_w} K_{2,FCN}(x_i, x'_i)$, where $K_{2,FCN}$ is the FCN kernel ($N_w = 1$). Focusing on a linear target for simplicity, we can work out the scaling of the relevant (linear) kernel feature by Taylor expanding $K_{2,FCN} = a_1 x_i \cdot x'_i / S$ to get $K_{2,CNN} = \frac{a_1}{N_w S} x \cdot x'$, with a_1 being some $\mathcal{O}(1)$ constant. Lazy learning then yields $\tilde{E}_{q \sim GP} = N_w S = d$, as in a FCN with no weight sharing.
- (2) **GFL:** Here, we take $\Sigma = I_S/S + D w_* w_*^\top$, resulting in $\Delta_{l=1} = ND$. The leading term of the Taylor expansion now equals $K_{2,CNN} = \frac{1}{N_w S} \sum_{i=1}^{N_w} x_i^\top \Sigma x'_i$ leading to a $D/(N_w S)$ scaling of the target. All in all, we find that $\tilde{E}_{q \sim GFL} = ND + (N_w S)/D$, leading to $\tilde{E}_{q_*} = \sqrt{NM_w S}$ for the optimal $q_* \sim GFL$.
- (3) **M-Specialization:** In this case, we obtain a $\Delta_{l=1} = MS$ cost. The contribution of the M specializing neurons to the kernel goes as $\frac{a_1 M}{N_w N} \sum_{i=1}^{N_w} (w_* \cdot x)(w_* \cdot x')$, leading to $a_y = \langle y, K_L, y \rangle = \mathcal{O}(M/N_w N)$. Thus, $\tilde{E}_{q \sim M\text{-Sp}} = MS + N_w N/M$ resulting in the optimal variational energy $\sqrt{SN_w N}$.

Both GFL and M-Specialization patterns, in the proportionate limit $N \propto N_w \propto S \rightarrow \infty$, lead to $P_* \propto S^{3/2} = d^{3/4}$. This recovers results reported in Ringel et al. [2025] computed via a mean-field approach.

E.2 Classification Tasks

We consider a fully connected network as defined in 78 with $N_w = 1$ and ReLU activations, trained on a k -parity classification task. Explicitly, this task is defined as-

$$y_k(x) = \text{sign} \prod_{j=1}^k x_j, \quad (79)$$

where $\eta \sim \mathcal{N}(0, 1)$, and for $i = 1, \dots, d$, $x_i = s_i + \mathcal{N}(0, \epsilon)$, for and s_i that are i.i.d. random binary values in $\{\pm 1\}$. We take cross-entropy loss, and consider $k = 2$.

Here we observe that the target is given by-

$$y_2(x) = \text{sign}((x_1 + \eta_1)(x_2 + \eta_2)) = \text{sign}(\frac{1}{2}(x_1 + x_2)^2 - x_1^2 - x_2^2) \quad (80)$$

This setting is similar to the previously discussed polynomial target in the erf networks. The difference in this case is that there are multiple relevant directions, namely: $w_{*,1} = \hat{e}_1, w_{*,2} = \hat{e}_2, w_{*,1+2} = \hat{e}_1 + \hat{e}_2$, and up to multiplicative constants on the target and constant additions. As in the previous cases, we compute the scale of the optimal variational energy for each pattern, and consider the same patterns as in the two layer network. In this case, we can further consider another setting of feature learning. Rather than taking M specializing neurons, and setting each of them to specialize with amplitude $\mu = 1$, we can set ≈ 1 neuron to specialize with magnitude μ . As the erf was a bounded activation, this choice was not beneficial in that case we did not need to consider it as well. Defining the last pattern as μ -Specialization, and comparing to the previously discussed patterns, we obtain:

- (1) **GP:** Here, $\Delta_{1,i} = 0$ since $K_{l-1} = Q_l$. As in the case of the erf network, we have $\tilde{E}_{q \sim \text{GP}} \propto d^2$.
- (2) **GFL:** Here we have $\tilde{E}_{q \sim \text{GFL}} \propto ND + (d/D)^2$. Minimizing w.r.t. D , we obtain $D_{\min} = d^{2/3}/N^{1/3}$, and, substituting back, we obtain $\tilde{E}_{q \sim \text{GFL}} \propto (Nd)^{\frac{2}{3}}$.
- (3) **M-Specialization:** $\tilde{E}_{q \sim \text{M-Sp}} \propto dM + N/M$. Minimizing further over M , the number of specializing neurons leads to $M_{\min} = \sqrt{N/d}$ and therefore $\tilde{E}_{q \sim \text{M-Sp}} \propto \sqrt{dN}$.
- (4) **μ -Specialization:** Following 10, and the second feature propagation rule, we obtain this pattern incurs a cost of $\Delta_1 = \mu^2 d$. Utilizing the first feature propagation rule, this pattern results in adding a spike of the kernel so that $a_y \propto N/\mu^2$, we obtain $\tilde{E}_{q \sim \text{M-Sp}} \propto d\mu^2 + N/\mu^2$. Minimizing further over μ , the magnitude of the specializing neurons leads to $\mu_{\min} = (N/d)^{1/4}$ and therefore $\tilde{E}_{q \sim \mu\text{-Sp}} \propto \sqrt{dN}$.

There is a redundancy in the preferential patterns, as both specialization distributions result in a variational energy that scales as $P_* \propto \sqrt{Nd}$. Experimentally, we find that indeed the feature learning patterns that emerge for this case correspond to μ -Specialization, with the correct scaling of the specialization magnitude with the layer width, as can be seen in 7.

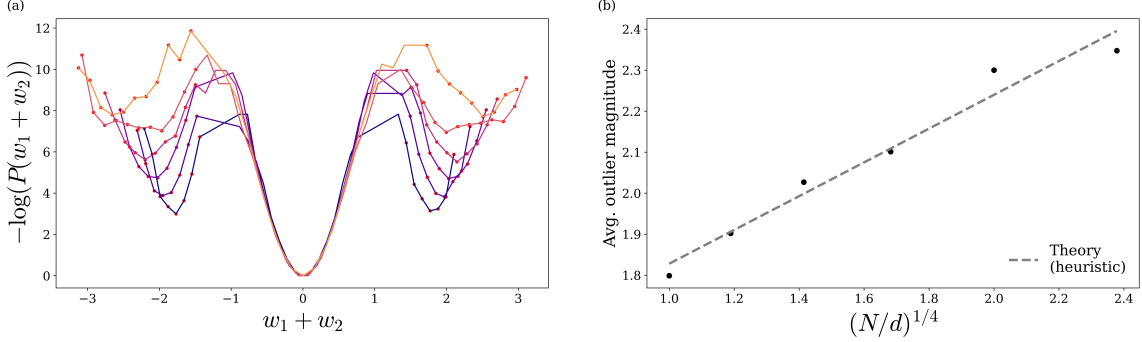


Figure 7: Emergence of specialization in two layer ReLU networks trained on classification task. In (a), the negative log distribution of the weights in the hidden layer in one of the feature directions is shown, with neurons classified as specializing appearing in red. Specifically, in this figure the distribution is shown for $w_{*,1+2}$. Although in this setting there are multiple relevant feature direction, we observe a similar μ -Specialization behavior in all of these. A single direction is considered here for simplicity. In (b) the magnitude of the specializing neuron as a function of the network width is shown. Indeed, our Heuristics manage to correctly predict the scaling of the learned feature with increasing here.

E.3 Softmax Attention Layer

Here, we consider an attention block of the form

$$f(X) = \frac{1}{\sqrt{L}} \sum_{h=1}^H \sum_{a,b=1}^L @_{ab;h}(X) (w_h \cdot x^b) \quad (81)$$

$$@_{ab;h}(X) = \frac{e^{[x^a]^\top A_h x^b}}{\sum_{c=1}^L e^{[x^a]^\top A_h x^c}}$$

where $X \in \mathbb{R}^{L \times d}$, $A_h \in \mathbb{R}^{d \times d}$, $x^a \in \mathbb{R}^d$ is the a -th row of X , and $w_h \in \mathbb{R}^d$. Our prior over network weights is $\prod_{h=1}^H \mathcal{N}[0, I_{d^2}/d^2; A_h] \mathcal{N}[0, I_d/(dH); w_h]$. The only context length (L) dependence comes from the pre-factor of $1/\sqrt{L}$ which ensures that when $X_i^a \sim \mathcal{N}(0, 1)$ then we have $f(X) = \mathcal{O}(1)$. We consider the target function $y(X) = \sum_{a,b} \frac{1}{\sqrt{L(L-1)}} x_1^a x_2^b x_3^b$.

As $H \rightarrow \infty$, the above $f(X)$ tends to a GP with w_h taking the role of read-out layer weights and a kernel given by

$$K(X, X') = (dL)^{-1} \sum_{a,a',b,b'=1}^L (x^b \cdot (x')^{b'}) \mathbb{E}_A [\@_{ab}(X) \@_{a'b'}(X')], \quad (82)$$

where we dropped the multi-head index h by our i.i.d. assumption.

Our goal is to find the sample complexity and scaling of feature learning effects with context length (L) at finite d . To this end, we shall consider the following weight-space version of \tilde{E} given

by,

$$\tilde{E}_q = \sum_{h=1}^H d^2 \mathbb{E}_{A_h \sim q_h} [Tr[A_h A_h^\top] - 1] + \frac{1}{\langle y, K, y \rangle}. \quad (83)$$

where K is computed using the q_h distribution for A . There are several ways of obtaining this variational energy; a direct microscopic route is shown in Sec. E.3.1. Alternatively, one can use the arguments of Sec. D, previously employed in Sec. E.1.2, and trade the kernel version of $\Delta_{l,i}$ with the excess weight decay of that layer. The latter being the first term in the above formula.

We will focus on two learning patterns here: lazy learning (GP) and weight specialization. For lazy learning, we take $q_h = \mathcal{N}[0, I_{d^2 \times d^2} / d^2; A_h]$ leading, as expected, to zero contribution from the first term in \tilde{E}_q .

To assess the scaling of $\langle y(X), K(X, X'), y(X') \rangle$ with L , we make the following observations. For large L and random A_h 's, the denominator of $\mathbb{Q}_{ab}(X)$ is $O(L)$ plus smaller fluctuations namely

$$\begin{aligned} \mathbb{Q}_{ab;h}(X) &= \frac{e^{[x^a]^\top A_h x^b}}{\sum_{c=1}^L e^{[x^a]^\top A_h x^c}} = \frac{e^{[x^a]^\top A_h x^b}}{Z + [\sum_{c=1}^L e^{[x^a]^\top A_h x^c} - Z]} \\ Z &= \mathbb{E}_A \left[\sum_{c=1}^L e^{[x^a]^\top A_h x^c} \right] = O(L) \end{aligned} \quad (84)$$

which allows an expansion in the small parameter $[\sum_{c=1}^L e^{[x^a]^\top A_h x^c} - Z]/Z = O(1/\sqrt{L})$. Next, we observe that functions involving l -sequence index functions, such as our $l = 2$ target, appear at $l - 2$ order of this expansion. Thus, we suffice with a leading order expansion

$$\begin{aligned} \langle f(X), y(X) \rangle &= \frac{1}{\sqrt{L}} \sum_{h=1}^H \left\langle Z^{-1} \sum_{ab=1}^L e^{[x^a]^\top A_h x^b} w_h \cdot x^b + O(L^{-1}), \sum_{c,d=1}^L \frac{1}{\sqrt{L(L-1)}} x_1^c x_2^d x_3^d \right\rangle \quad (85) \\ &= \frac{1}{\sqrt{L}} \sum_{h=1}^H \left\langle Z^{-1} \sum_{ab=1}^L e^{[x^a]^\top A_h x^b} w_h \cdot x^b + O(L^{-1}), \frac{1}{\sqrt{L(L-1)}} x_1^a x_2^b x_3^b \right\rangle = \dots \end{aligned}$$

where we used the fact that, under our Gaussian measure, $x_2^d x_3^d$ projects out any term which does not contain an odd power of x_2^b and an odd power of x_3^b and a similar consideration with x_1^a . Next, a direct computation gives

$$\begin{aligned} \dots &= \frac{1}{\sqrt{L^2(L-1)}Z} \sum_{h=1}^H Z^{-1} \sum_{ab=1}^L ([A_h]_{12}[w_h]_3 + [A_h]_{13}[w_h]_2 (1 + O(Tr[A_h A_h^\top])) + O([A_h A_h^\top A_h]_{12}[w_h]_3) + O(A^5)) \\ &\quad + O(L^{-1}) = \dots \end{aligned} \quad (86)$$

Noting that under our distribution for A , $Tr[AA^\top] = O(1)$ and $O([A_h A_h^\top A_h]_{ij}) = O([A_h]_{ij})$ we finally obtain that the typical scale of the r.h.s. the same as its leading order expansion in A namely

$$\dots \propto \frac{\sqrt{L}}{Z} \sum_{h=1}^H ([A_h]_{12}[w_h]_3 + [A_h]_{13}[w_h]_2) \quad (87)$$

Finally, computing $\langle y(X), K(X, X'), y(X') \rangle$ amount to computing the 2nd moment of the above term under the prior for A_h, w_h which, given that $Z = O(L)$, yields a scaling

$$\langle y, K, y \rangle \propto \frac{1}{Ld^3} \quad (88)$$

Implying that $\tilde{E}_{\text{lazy}} \propto Ld^3$.

We next consider a specializing scenario ($q_{sp.}$) where for $O(1)$ heads, $[A_h]_{12}$ has an average of the order M/d . Other components of A_h as well as A_h 's of the remaining heads, remain lazy. The motivation for this choice, also observed empirically, is that together with a spike in $[w_h]_3$, one can create strong alignment in Eq. (87). Other combinations of 1, 2, 3 indices are also possible and lead to the same scaling.

Using the above $q_{sp.}$, the excess weight-decay (first term in \tilde{E}_q) gets contributions only from the $O(1)$ specializing heads scaling as $d^2(M/d)^2$. One further notes that using this A_{12} , in Eq. 87 and subsequently in 88, yields $\langle y, K, y \rangle \propto \frac{M^2/d^2}{LdH}$ leading to $\tilde{E}_{sp.} = M^2 + HLd^3/M^2$. Optimizing the latter over M^2 leads to $\tilde{E}_{sp,opt} = \sqrt{Ld^3}d^{1.5}$. This scenario is thus favorable to lazy learning up to $H = O(\sqrt{Ld^3})$.

To validate these results, we consider the above model, with $d = 8$ and $d = 16$, $H = 2$, $\kappa = 0.1$, and $P = 350, 500, 707, 1000$ data points, and a maximal context length of $180, 360, 720, 720$ respectively. Fig. 3(b) shows target alignment of the equilibrated network as a function of $\sqrt{Ld^3}/P$, demonstrating that $P = \sqrt{Ld^3}$ is the scale at which $O(1)$ alignment appears. A similar plot for the Test MSE results is shown in the right panel.

E.3.1 Direct derivation of \tilde{E}_q for a softmax block

Gathering all A_h, w parameters into Θ , the probability of alignment α is given by

$$p_{A_f}(\alpha) = \frac{1}{2\pi} \int dt \int d\Theta p(\Theta) \exp(it(\langle y, f_\Theta \rangle - \alpha)). \quad (89)$$

We can integrate out w_h as follows:

$$p_{A_f}(\alpha) = \frac{1}{2\pi} \int dt \int d\Theta p(\Theta) \exp \left(it \left(\left\langle y, \frac{1}{\sqrt{L}} \sum_{h=1}^H \sum_{a,b=1}^L @_{ab;h}(x)(w_h \cdot x^b) \right\rangle - \alpha \right) \right).$$

Let $v_h(x) := \sum_{b=1}^L (\sum_{a=1}^L @_{ab;h}(x)) x^b$. Then, we can re-write

$$\begin{aligned} p_{A_f}(\alpha) &= \frac{1}{2\pi} \int dt \int d\Theta p(\Theta) \exp \left(it \left(\frac{1}{\sqrt{L}} \sum_{h=1}^H \langle y, w_h \cdot v_h \rangle - \alpha \right) \right) \\ &= \frac{1}{2\pi} \int dt \int d\Theta p(\Theta) \exp \left(it \left(\frac{1}{\sqrt{L}} \sum_{h=1}^H w_h \cdot \langle y, v_h \rangle - \alpha \right) \right) \end{aligned}$$

where we're using an unusual notation, regarding $\langle y, v_h \rangle$ as a vector of L_2 inner products. Using the prior we continue:

$$\begin{aligned}
&= \frac{1}{2\pi} \int dt \exp(-ita) \prod_{h=1}^H \int dA_h p(A_h) \int dw_h p(w_h) \exp\left(\frac{it}{\sqrt{L}} w_h \cdot \langle y, v_h \rangle\right) \\
&= \frac{1}{2\pi} \int dt \exp(-ita) \prod_{h=1}^H \int dA_h p(A_h) \exp\left(-\frac{1}{2} \frac{t^2}{LdH} \langle y, v_h \rangle^\top \langle y, v_h \rangle\right) \\
&= \frac{1}{2\pi} \int dA p(A) \int dt \exp\left(-\frac{1}{2} \frac{t^2}{LdH} \sum_{h=1}^H \langle y, v_h \rangle^\top \langle y, v_h \rangle - it\alpha\right)
\end{aligned}$$

When we integrate out t we get

$$\begin{aligned}
p_{A_f}(\alpha) &= \\
&= \frac{1}{\sqrt{2\pi}} \int dA p(A) \exp\left(-\frac{\alpha^2}{\frac{2}{LdH} \sum_{h=1}^H \langle y, v_h \rangle^\top \langle y, v_h \rangle} + \frac{1}{2} \log \frac{1}{\frac{1}{LdH} \sum_{h=1}^H \langle y, v_h \rangle^\top \langle y, v_h \rangle}\right)
\end{aligned} \tag{90}$$

Let's denote

$$\kappa(A) := \frac{1}{LdH} \sum_{h=1}^H \langle y, v_h \rangle^\top \langle y, v_h \rangle = \frac{1}{LdH} \sum_{h=1}^H \sum_{i=1}^d \langle y, [v_h]_i \rangle^2.$$

Then we have

$$\begin{aligned}
p_{A_f}(\alpha) &= \int dA p(A) \frac{1}{\sqrt{2\pi\kappa(A)}} \exp\left(-\frac{\alpha^2}{2\kappa(A)}\right) \\
&= \int dA p(A) \mathcal{N}(0, \kappa(A); \alpha)
\end{aligned}$$

Next, we take a layer-decoupling approximation, similar in spirit to kernel adaptation, where we assume $\kappa(A)$ does not fluctuate out of scale, with A . We thus trade $\kappa(A)$ by its average, which yields our a_y term, $\alpha^2/\langle y, K, y \rangle$. As in the original derivation, we expect a_y to be extensive ($O(d, N, \dots)$) and hence its log, or equivalently the above $1/\sqrt{2\pi\kappa(A)}$ prefactor of the exponent is negligible. The action (S), or negative log-probability associated with $p(A)e^{-\alpha^2/(2\kappa(A))}$ is now given by $S = (d^2 \text{Tr}[A^T A] + \alpha^2/\kappa(A))/2$. Using a variational principle on this action with a Gaussian q , one obtains the above variational energy, with the $-d^2$ contribution coming from the entropy term $\int dA q(A) \log(q(A))$ in the KL-divergence used in the variational approach (similarly to how $-H_{q,\alpha}(h)$ emerged in sec. C.2)

F Experimental details

F.0.1 Two-layer FCN- Experimental Details

In panels (a) and (b) of Fig. 2, the experimental data points were computed by training an ensemble of 300 networks. For panel (a), all experiments used $P = 40d$ and $N = d = 40$, with a ridge

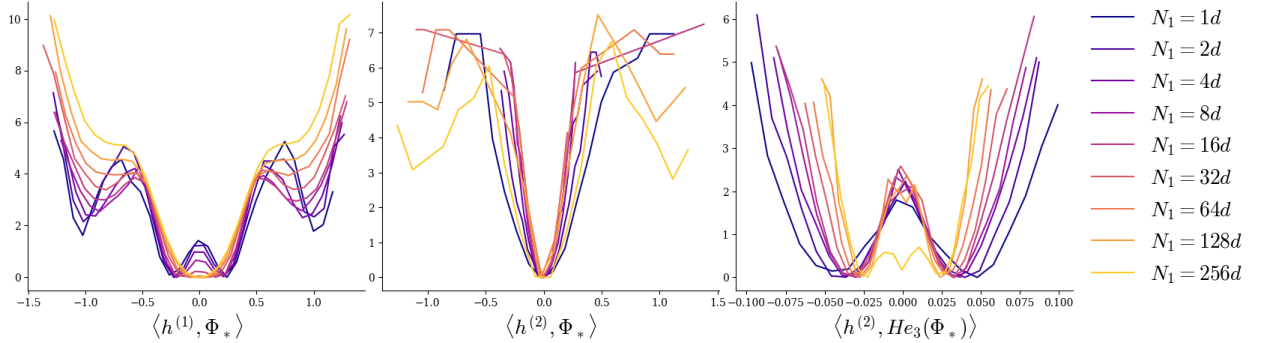


Figure 8: Distribution of pre-activations of the alignment of the first and second layers with the linear feature- $\Phi_* = w_* \cdot x$, and the cubic feature- $\hat{He}_3(\Phi_*)$ where the hat simply denotes the normalized third Hermite polynomial. As can be seen in this figure, increasing the width of the first layer- N_1 pushes the preferred feature learning pattern, from Specialization-magnetization to GP-Specialization, as predicted by the our approach.

parameter of 1 and variances of $\sigma_1^2 = \sigma_2^2 = 1$. For panel (b), we set $N = d$ while varying both d and P . The experimental value of P_* was calculated by extrapolating from the different values of P and their corresponding alignments, and then inverting this correspondence to find the value of P for which $A_f = 0.1$.

In panel (c), we set $P = 40d$ and $d = 40$, while increasing the value of N . As in the other panels, we used $\sigma_1^2 = \sigma_2^2 = 1$, but here we set the ridge parameter to $\kappa = 0.25$. We trained an ensemble of 300 networks and computed a histogram of the pre-activation alignment in the hidden layer. First-layer outliers were defined as any pre-activations having an overlap with $\Phi_*(x) = w_* \cdot x$ of more than $3\sigma_1/\sqrt{d}$ (three times the standard deviation of the GP distribution). The total number of such outliers was counted and then averaged over the ensemble of networks.

F.1 Three-layer FCN- Experimental Details

In panel (a) of Fig. 3, the experimental data was computed by training an ensemble of 30 networks. For all experiments, we set $d = N_1 = N_2$, with a ridge parameter of 0.125 and variances of $\sigma_1^2 = \sigma_2^2 = 0.25$.

For panel (c) of Fig. 3 and in Fig. 8, we set $P = 40d$ and $d = N_2 = 10$, while increasing the value of N_1 . We further used $\sigma_1^2 = \sigma_2^2 = 0.25$ and a ridge parameter of $\kappa = 0.125$. An ensemble of 300 networks was trained to compute the following histograms for the pre-activation alignments: 1. of the linear feature in the first hidden layer, 2. with the linear feature in the second layer, and 3. with the target in the second layer. Outliers in the first layer were calculated as in the two-layer case. For the second layer, activation alignments deviating by more than 3 times the NNGP standard deviation were considered outliers.

F.2 Alignment as a tight bound on MSE

A central component of our approach is using alignment as a certificate for good learning. As discussed in the main body of the text, the alignment is indeed a lower bound on the MSE through

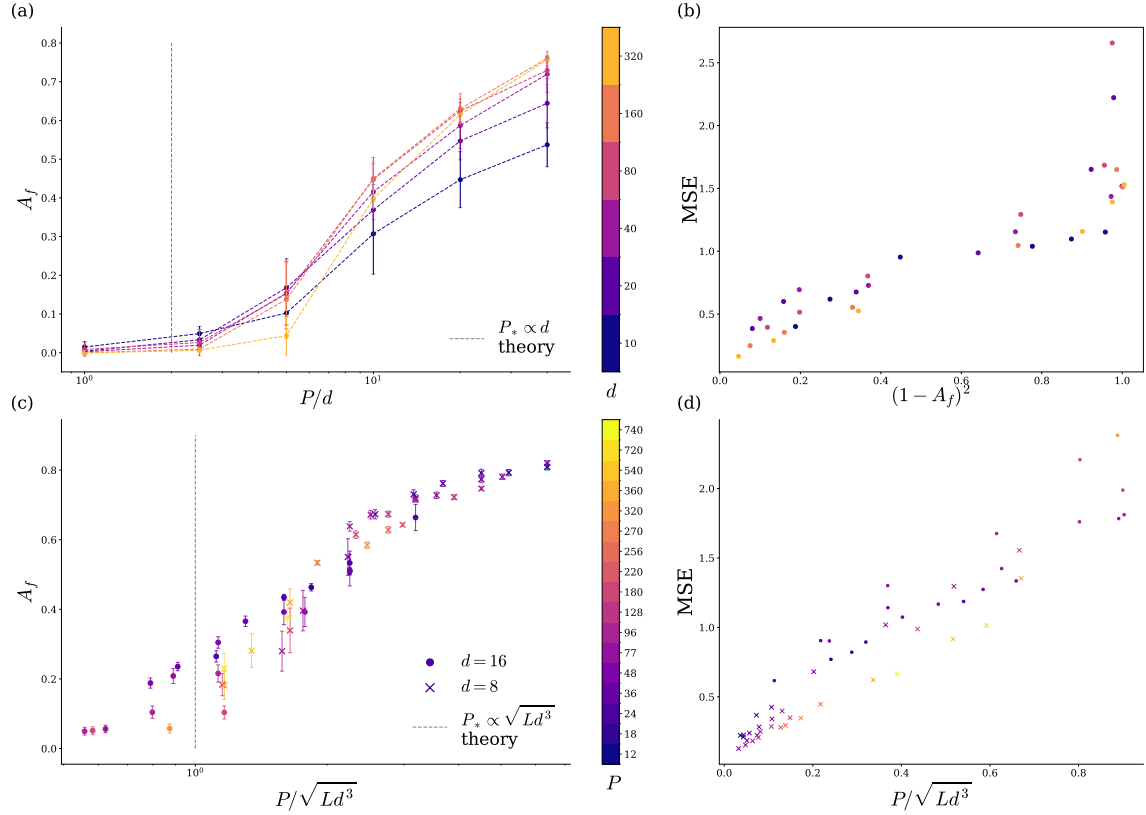


Figure 9: Evidence that alignment is a tight lower bound on MSE. Here we provide results from two experiments, softmax attention (panels (c) and (d)), and three layer network (panels (a) and (b)). These results clearly imply that the alignment is a strong indicator of good MSE.

the inequality $\text{MSE} \geq (1 - A_f)^2$. However, this inequality does not necessitate that the MSE will vanish. We therefore provide in this section empirical evidence that strong alignment is indeed an indication of MSE. To this extent, we provide results both from the softmax attention experiments and the three layer case, and in both we find that strong alignment is closely correlated with low loss, as can be seen in Fig.

G Comparing Kernel Adaptation and LDT

The results in the heuristic approach presented here are closely related to the kernel adaptation approach Fischer et al. [2024], Seroussi et al. [2023b], Ringel et al. [2025], Rubin et al. [2024, 2025]. In this section, we compute explicitly the mean posterior predictor for the alignment. Interestingly, we find that the equations for the LDT approach are remarkably similar to those of the mean predictor.

As in the derivation of the Chernhoff bounds we begin by integrating out the readout weights

from the posterior, and introducing a delta function Fourier field in the prior, we obtain-

$$Z = \int d\tilde{t} \int d\Theta^{L-1} p(\Theta^{L-1}) \exp \left(-\frac{\sigma_L^2}{2N_L \chi} \sum_{i=1}^{N_L} \langle \sigma(h_i^{L-1}(x)), \tilde{t}(x) \rangle^2 - \frac{\kappa}{2} \langle \tilde{t}, \tilde{t} \rangle + i \langle y, \tilde{t} \rangle \right) \quad (91)$$

where \tilde{t} is an imaginary helper field originating from the delta function. Define-

$$\tilde{t}(x) = t_y y(x) + t_{\perp} y_{\perp}(x) \quad (92)$$

where y_{\perp} is some function that is orthogonal to y , so that $\langle y, y_{\perp} \rangle = 0$. Now we have-

$$\begin{aligned} Z = & \int dt_y dt_{\perp} \exp \left(-\frac{\kappa}{2} (t_y^2 + t_{\perp}^2) + it_y \right) \int d\Theta^{L-1} p(\Theta^{L-1}) \\ & \cdot \exp \left(-\sum_{i=1}^{N_L} \frac{\sigma_L^2}{2N_L} (t_y \langle y(x), \sigma(h_i^{L-1}(x)) \rangle + t_{\perp} \langle y_{\perp}(x), \phi(w_i \cdot x) \rangle)^2 \right) \end{aligned} \quad (93)$$

Next, we assume self consistently that t_{\perp} vanishes, and so the above equation simplifies to:

$$Z = \int dt_y dt_{\perp} \exp \left(-\frac{\kappa}{2} \left(t_y - \frac{i}{\kappa} \right)^2 \right) \int d\Theta^{L-1} p(\Theta^{L-1}) \exp \left(-\sum_{i=1}^{N_L} \frac{\sigma_L^2}{2N_L} t_y^2 \underbrace{\langle y(x), \sigma(h_i^{L-1}(x)) \rangle^2}_{a_i(\Theta^{L-1})} \right) \quad (94)$$

Here enters the adaptive approach. We assume that t_y is weakly fluctuating, and approximate-

$$\exp \left(\frac{\sigma_a^2}{2N} t_y^2 A_i^2 \right) \approx \exp \left(-\sum_{i=1}^{N_L} \frac{\sigma_L^2}{2N_L} \mathbb{E}_{t_y} [t_y^2] a_i^2(\Theta^{L-1}) + \sum_{i=1}^{N_L} \frac{\sigma_L^2}{2N_L} t_y^2 \mathbb{E}_{\Theta^{L-1}} [a_i^2] \right) \quad (95)$$

So that

$$\begin{aligned} Z \propto & \int dt_y \exp \left(\underbrace{-\frac{\kappa}{2} \left(t_y - \frac{i}{\kappa} \right)^2 - \sum_{i=1}^{N_L} \frac{\sigma_L^2}{2N_L} t_y^2 \mathbb{E}_{\Theta^{L-1}} [a_i^2]}_{:= -S_{t_y}} \right) \\ & \cdot \int d\Theta^{L-1} \exp \left(\underbrace{-\sum_{i=1}^{N_L} \frac{\sigma_L^2}{2N_L} \mathbb{E}_{t_y} [t_y^2] a_i^2(\Theta^{L-1}) + \log p(\Theta^{L-1})}_{:= -S_{\Theta^{L-1}}} \right) \end{aligned} \quad (96)$$

We require self consistently that $\mathbb{E}_{\Theta^{L-1}} [a_i(\Theta^{L-1})]$ is indeed given by the expectation with respect to the action $S_{\Theta^{L-1}}$

$$\begin{aligned} & \mathbb{E}_{\Theta^{L-1}} [a_j(\Theta^{L-1})] = \mathbb{E}_{\Theta^{L-1} \sim S_{\Theta^{L-1}}} [a_j(\Theta^{L-1})] \quad (97) \\ & = \frac{\int d\Theta^{L-1} p(\Theta^{L-1}) a_j(\Theta^{L-1}) \exp \left(-\frac{\sigma_L^2}{2N_L} \mathbb{E}_{t_y} [t_y^2] \sum_{i=1}^{N_L} a_i(\Theta^{L-1}) \right)}{\int d\Theta^{L-1} p(\Theta^{L-1}) \exp \left(-\sum_{i=1}^{N_L} \frac{\sigma_L^2}{2N_L} \mathbb{E}_{t_y} [t_y^2] \sum_{i=1}^{N_L} a_i(\Theta^{L-1}) \right)} \end{aligned}$$

Denoting- $\sum_{i=1}^{N_{L-1}} a_i(\Theta^{L-1}) := a(\Theta^{L-1})$, and $\int d\Theta^{L-1} p(\Theta^{L-1})(...) = \mathbb{E}_{\Theta^{L-1} \sim \text{GP}}[(...)]$, then we have-

$$\begin{aligned} \sum_{j=1}^{N_L} \mathbb{E}_{\Theta^{L-1} \sim S_{\Theta^{L-1}}} [a_j(\Theta^{L-1})] &:= \mathbb{E}_{\Theta^{L-1} \sim S_{\Theta^{L-1}}} [a(\Theta^{L-1})] \\ &= \frac{\mathbb{E}_{\Theta^{L-1} \sim \text{GP}} \left[a(\Theta^{L-1}) \exp \left(-\frac{\sigma_L^2}{2N_L} \mathbb{E}_{t_y} [t_y^2] a(\Theta^{L-1}) \right) \right]}{\mathbb{E}_{\Theta^{L-1} \sim \text{GP}} \left[\exp \left(-\frac{\sigma_L^2}{2N_L} \bar{t}_y^2 a(\Theta^{L-1}) \right) \right]} \end{aligned} \quad (98)$$

Next we require that the same condition holds for t_y . Note that the action for t_y is simply a Gaussian one, and following square completion we have-

$$e^{-S_{t_y}} \propto \exp \left(-\frac{\left(\kappa + \frac{\sigma_L^2}{N_L} \mathbb{E}_{\Theta^{L-1}} [a(\Theta^{L-1})] \right)}{2} \left(t_y - \frac{i}{\left(\kappa + \frac{\sigma_L^2}{N_L} \mathbb{E}_{\Theta^{L-1}} [a(\Theta^{L-1})] \right)} \right)^2 \right) \quad (99)$$

So that

$$t_y \sim \mathcal{N} \left(i \left(\kappa + \frac{\sigma_L^2}{N_L} \mathbb{E}_{\Theta^{L-1}} [a(\Theta^{L-1})] \right)^{-1}, \left(\kappa + \frac{\sigma_L^2}{N_L} \mathbb{E}_{\Theta^{L-1}} [a(\Theta^{L-1})] \right)^{-1} \right) \quad (100)$$

So that we can substitute the self consistency requirement on the Θ variables into the expression for the mean of t_y and we obtain

$$\mathbb{E}_{t_y \sim S_{t_y}} [t_y] = i \left(\kappa + \frac{\frac{\sigma_L^2}{N_L} \mathbb{E}_{\Theta^{L-1} \sim \text{GP}} \left[a(\Theta^{L-1}) \exp \left(-\frac{\sigma_L^2}{2N_L} \mathbb{E}_{t_y \sim S_{t_y}} [t_y^2] a(\Theta^{L-1}) \right) \right]}{\mathbb{E}_{\Theta^{L-1} \sim \text{GP}} \left[\exp \left(-\frac{\sigma_L^2}{2N_L} \mathbb{E}_{t_y \sim S_{t_y}} a(\Theta^{L-1}) \right) \right]} \right)^{-1}$$

Note that if we approximate- $\mathbb{E}_{t_y \sim S_{t_y}} [t_y^2] \sim \mathbb{E}_{t_y \sim S_{t_y}}^2 [t_y]$, then we obtain a self consistent equation for $\mathbb{E}_{t_y \sim S_{t_y}} [t_y] := \bar{t}_y$, given by-

$$\bar{t}_y = \frac{i \mathbb{E}_{\Theta^{L-1} \sim \text{GP}} \left[\exp \left(-\frac{\sigma_L^2}{2N_L} \bar{t}_y^2 a(\Theta^{L-1}) \right) \right]}{\mathbb{E}_{\Theta^{L-1} \sim \text{GP}} \left[\left(\kappa + \frac{\sigma_L^2}{N_L} a(\Theta^{L-1}) \right) \exp \left(-\frac{\sigma_L^2}{2N_L} \bar{t}_y^2 a(\Theta^{L-1}) \right) \right]} \quad (101)$$

Rewriting with real $\bar{t}_y \mapsto i\bar{t}_y$, we obtain the self consistency equation-

$$\bar{t}_y = \frac{\mathbb{E}_{\Theta^{L-1} \sim \text{GP}} \left[\exp \left(\frac{\sigma_L^2}{2N_L} \bar{t}_y^2 a(\Theta^{L-1}) \right) \right]}{\mathbb{E}_{\Theta^{L-1} \sim \text{GP}} \left[\left(\kappa + \frac{\sigma_L^2}{N_L} a(\Theta^{L-1}) \right) \exp \left(\frac{\sigma_L^2}{2N_L} \bar{t}_y^2 a(\Theta^{L-1}) \right) \right]} \quad (102)$$

Replacing $\tilde{a} = \kappa + \frac{\sigma_L^2}{N_L} a(\Theta^{L-1})$, we obtain the following self consistent equation for \bar{t}_y :

$$\bar{t}_y = \frac{\mathbb{E}_{\Theta^{L-1} \sim \text{GP}} \left[\exp \left(\frac{\sigma_L^2}{2N_L} \bar{t}_y^2 \tilde{a}(\Theta^{L-1}) \right) \right]}{\mathbb{E}_{\Theta^{L-1} \sim \text{GP}} \left[\left(\frac{\sigma_L^2}{N_L} \tilde{a}(\Theta^{L-1}) \right) \exp \left(\frac{\sigma_L^2}{2N_L} \bar{t}_y^2 \tilde{a}(\Theta^{L-1}) \right) \right]} \quad (103)$$

This expression is very similar to the one we found for the upper Chernoff bound, and the two equations coincide in the limit $\kappa \rightarrow 0$, and $\alpha \rightarrow 1$.